iScience

CellPress
OPEN ACCESS

Article

LIFR-α-dependent adipocyte signaling in obesity limits adipose expansion contributing to fatty liver disease

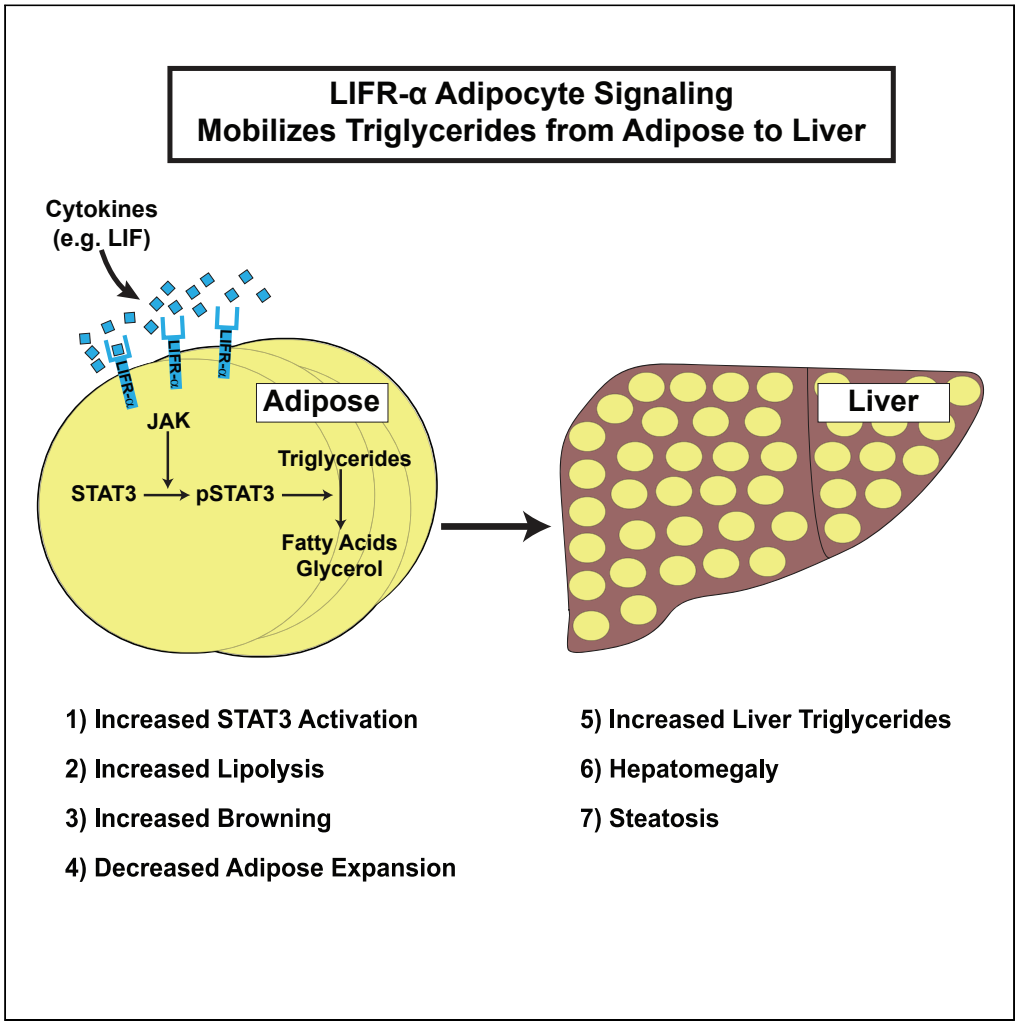

Tong Guo, Arun Gupta, Jinhai Yu, ..., Bret M. Evers, Puneeth Iyengar, Rodney E. Infante

puneeth.iyengar@utsouthwestern.edu (P.I.)
rodney.infante@utsouthwestern.edu (R.E.I.)

HIGHLIGHTS

LIFR-α signaling induces adipocyte lipolysis, restricting adipose expansion in DIO

LIFR-α signaling requires STAT3 for adipocyte lipolysis

LIFR-α/JAK/STAT3 lipolysis signaling in adipocytes promotes hepatic steatosis

Guo et al., iScience *24*, 102227
March 19, 2021
https://doi.org/10.1016/j.isci.2021.102227

iScience

CellPress
OPEN ACCESS

Article

LIFR-α-dependent adipocyte signaling in obesity limits adipose expansion contributing to fatty liver disease

Tong Guo,[1,2,7] Arun Gupta,[3,7] Jinhai Yu,[1,2] Jorge Z. Granados,[1] Aakash Y. Gandhi,[1,4] Bret M. Evers,[5] Puneeth Iyengar,[1,3,4,*] and Rodney E. Infante[1,2,4,6,8,*]

SUMMARY

The role of chronic adipose inflammation in diet-induced obesity (DIO) and its sequelae including fatty liver disease remains unclear. Leukemia inhibitory factor (LIF) induces JAK-dependent adipocyte lipolysis and altered adipo/cytokine expression, suppressing *in vivo* adipose expansion in normal and obese mouse models. To characterize LIF receptor (LIFR-α)-dependent cytokine signaling in DIO, we created an adipocyte-specific *LIFR* knockout mouse model (*Adipoq-Cre;-LIFR*$^{fl/fl}$). Differentiated adipocytes derived from this model blocked LIF-induced triacylglycerol lipolysis. *Adipoq-Cre;LIFR*$^{fl/fl}$ mice on a high-fat diet (HFD) displayed reduced adipose STAT3 activation, 50% expansion in adipose, 20% body weight increase, and a 75% reduction in total hepatic triacylglycerides compared with controls. To demonstrate that LIFR-α signals adipocytes through STAT3, we also created an *Adipoq-Cre;STAT3*$^{fl/fl}$ model that showed similar findings when fed a HFD as *Adipoq-Cre;LIFR*$^{fl/fl}$ mice. These findings establish the importance of obesity-associated LIFR-α/JAK/STAT3 inflammatory signaling in adipocytes, blocking further adipose expansion in DIO contributing to ectopic liver triacylglyceride accumulation.

INTRODUCTION

An enrichment of immune factors and cells in adipose is associated with obesity, but their role in the development of obesity and the subsequent metabolic sequelae remains less understood (Bischoff et al., 2016; Cohen et al., 2011; Milano et al., 2020; Reilly and Saltiel, 2017; Van Pelt et al., 2017). Since the identification of secreted cytokine mediators of inflammation (e.g., TNFα, IL-1β, and IL-6), there has been an effort to connect signaling between these cytokines and the different cells within adipose tissue including adipocytes and stromal, vascular, and immune cells (Ferrante, 2013; Han et al., 2020; Kosteli et al., 2010; Lumeng et al., 2007a, 2007b, 2008). It is still uncertain, however, whether chronic adipose inflammation is a cause or a consequence of obesity. Furthermore, it is also not well understood if inflammation contributes to obesity's metabolic sequelae including non-alcoholic fatty liver disease (NAFLD), also referred to as metabolic-associated fatty liver disease (Cohen et al., 2011; Eslam et al., 2020). This ambiguity with obesity-associated adipose inflammation is underscored by the failure of multiple clinical trials to suppress obesity development and associated co-morbidities by targeting inflammatory molecules including TNFα and IL-1β (Reilly and Saltiel, 2017).

Leukemia inhibitory factor (LIF) is a member of the IL-6 family of inflammatory cytokines (Metcalf, 1991). LIF and IL-6 are both increased locally in adipose tissue and systemically in pre-clinical models and patients with obesity (Oñate et al., 2013; Roytblat et al., 2000; Yeste et al., 2007). These cytokines are also associated with adipose inflammation in cachexia, a syndrome on the opposite end of the metabolic spectrum (Arora et al., 2018; Auernhammer and Melmed, 2000; Seto et al., 2015). LIF signals through its canonical receptor LIFR-α (*LIFR* gene) and co-receptor gp130 to activate the JAK/STAT inflammatory pathway (Arora et al., 2018, 2020; Song and Lim, 2006). LIF signaling in differentiated adipocytes leads to JAK-dependent STAT3 phosphorylation, which (1) increases basal level lipolysis to break down triacylglycerol (TAG) to glycerol and fatty acids and (2) increases expression of the gene encoding IL-6 (*IL6*). Although STAT3 phosphorylation is associated with IL-6 family-mediated lipolysis, its role in transmitting these cytokine signals in the

[1]Center for Human Nutrition, University of Texas Southwestern Medical Center, 5300 Harry Hines Boulevard, Dallas, TX, USA

[2]Department of Molecular Genetics, University of Texas Southwestern Medical Center, Dallas, TX, USA

[3]Department of Radiation Oncology, University of Texas Southwestern Medical Center, Dallas, TX, USA

[4]Harold C. Simmons Comprehensive Cancer Center, University of Texas Southwestern Medical Center, Dallas, TX, USA

[5]Department of Pathology, University of Texas Southwestern Medical Center, Dallas, TX, USA

[6]Department of Internal Medicine, University of Texas Southwestern Medical Center, Dallas, TX, USA

[7]These authors contributed equally

[8]Lead contact

*Correspondence: puneeth.iyengar@utsouthwestern.edu (P.I.), rodney.infante@utsouthwestern.edu (R.E.I.)

https://doi.org/10.1016/j.isci.2021.102227

adipocyte has not been established. Recombinant LIF (rLIF) administered to mice, including models of obesity, limits further adipose expansion leading to a decrease in adipose and body weight due to anorexia and adipocyte lipolysis signals that are in part due to JAK-dependent adipose inflammation (Arora et al., 2018, 2020). These wasting effects do not require IL-6 because rLIF treatment of global *IL6* knockout mice yielded similar findings. The global murine *LIFR-α* knockout model is perinatal lethal, and no group has created an adipocyte-specific or inducible knockout model to define its role in adipose inflammation (Ware et al., 1995).

To better understand the role of LIF-induced adipose signaling during metabolic stress, we created an *Adipoq-Cre;LIFR*$^{fl/fl}$ mouse model. Compared with littermate controls, differentiated adipocytes derived from this model suppressed LIF-induced increases in lipolysis. The effect of ablating *LIFR* in adipocytes did not affect lipolysis by IL-6 and non-cytokine agonists, isoproterenol and forskolin derivative NKH477. Under the metabolic stress of a high-fat diet (HFD), the *Adipoq-Cre;LIFR*$^{fl/fl}$ mice had reduced STAT3 activation resulting in an ~20% increase in average adipocyte diameter, a 50% increase in adipose mass, and a 20% increase in body weight compared with littermate controls. Conversely, these mice demonstrated ~4-fold decrease in total hepatic TAGs during times of adipose expansion. To determine if LIFR-α-dependent adipose inflammatory signals require transduction through STAT3, we also created adipocyte-specific *STAT3* knockout (*Adipoq-Cre;STAT3*$^{fl/fl}$) mice. Similar to adipocytes from *Adipoq-Cre;LIFR*$^{fl/fl}$ mice, differentiated adipocytes derived from *Adipoq-Cre;STAT3*$^{fl/fl}$ mice were also able to suppress cytokine (LIF and IL-6)-induced increases in basal lipolysis. *Adipoq-Cre;STAT3*$^{fl/fl}$ mice displayed nearly identical findings to *Adipoq-Cre;LIFR*$^{fl/fl}$ mice during diet-induced obesity (DIO)—larger adipocyte sizes, greater adipose expansion, and less NAFLD—supporting STAT3's downstream role in LIFR-α-directed adipose signaling. Ultimately, this study defines the importance of the LIFR-α/JAK/STAT3 inflammatory signaling axis in adipocytes in suppressing adipose expansion by increasing the lipolytic potential, resulting in the development of NAFLD.

RESULTS

LIF-LIFR-α signaling induces adipocyte STAT3 activation and lipolysis

To understand the role of LIFR-α-dependent adipose signaling during metabolic stress, we created an adipocyte-specific *LIFR* knockout (*Adipoq-Cre;LIFR*$^{fl/fl}$) using the schema in Figure 1A. We conducted PCR of genomic DNA obtained from skin, epididymal white adipose tissue (eWAT), liver, and hypothalamus to verify that *LIFR* was only disrupted in adipose tissue (Figure 1A). In Figure 1B, we showed by qRT-PCR of the eWAT that expression of the gene encoding LIFR-α (*LIFR*) was reduced by 50% in the *Adipoq-Cre;LIFR*$^{fl/fl}$ mice compared with *LIFR*$^{fl/fl}$ littermate controls. In contrast, we identified no changes in expression of the genes encoding the cyto/adipokines IL-6 (*IL6*), LIF, or leptin (*Lep*). To isolate cells in adipose tissue that express adiponectin (adipocytes) from cells that do not express adiponectin (immune, vascular, and stromal), we separated *Adipoq-Cre;LIFR*$^{fl/fl}$ and littermate control eWAT adipocytes from their stromal vascular fraction (SVF). The adipocyte fractions were subjected to qRT-PCR, and *Adipoq-Cre;LIFR*$^{fl/fl}$ adipocytes demonstrated no detectable mRNA expression of *LIFR*, verifying disruption of the gene in adipocytes in the adipose tissue of the knockout animals (Figure 1C). Adipocytes from the *LIFR* knockout mice also had a significant decrease in *IL6* expression compared with littermate controls, which is consistent with our previous findings that LIF increases *IL6* expression in a JAK-dependent manner in differentiated adipocytes (Arora et al., 2020). At the protein level, there was a significant reduction in LIFR-α in eWAT of knockout mice compared with controls, with equivalent hepatic levels of LIFR-α in knockout and littermate controls (Figure 1D). Again, when we separated adipocytes from SVF cells, there was no LIFR-α protein expression in the adipocyte fraction of the *Adipoq-Cre;LIFR*$^{fl/fl}$ mice as judged by immunoblot analysis (Figure 1D, *isolated adipocytes*). These results validated our mouse model as a true adipocyte-specific knockout for *LIFR*.

To assess if LIFR-α is critical for transducing cytokine-mediated lipolysis signals, we differentiated adipocytes from the SVFs of *Adipoq-Cre;LIFR*$^{fl/fl}$ mice and littermate controls and conducted TAG lipolysis assays, non-esterified fatty acid (NEFA) release, and glycerol release, in the absence or presence of non-cytokines (isoproterenol, NKH477) or cytokines (IL-6 and LIF). Isoproterenol binds the GPCR β-adrenergic receptor activating adenylate cyclase to increase cAMP-mediated lipolysis (Arner, 1976; Vaughan and Steinberg, 1963). NKH477 is a forskolin derivative that directly activates adenylate cyclase, increasing cAMP to increase lipolysis, bypassing the β-adrenergic receptor (Yin et al., 2003). We next conducted lipolysis assays with increasing concentrations of compounds or cytokines using *Adipoq-Cre;LIFR*$^{fl/fl}$-

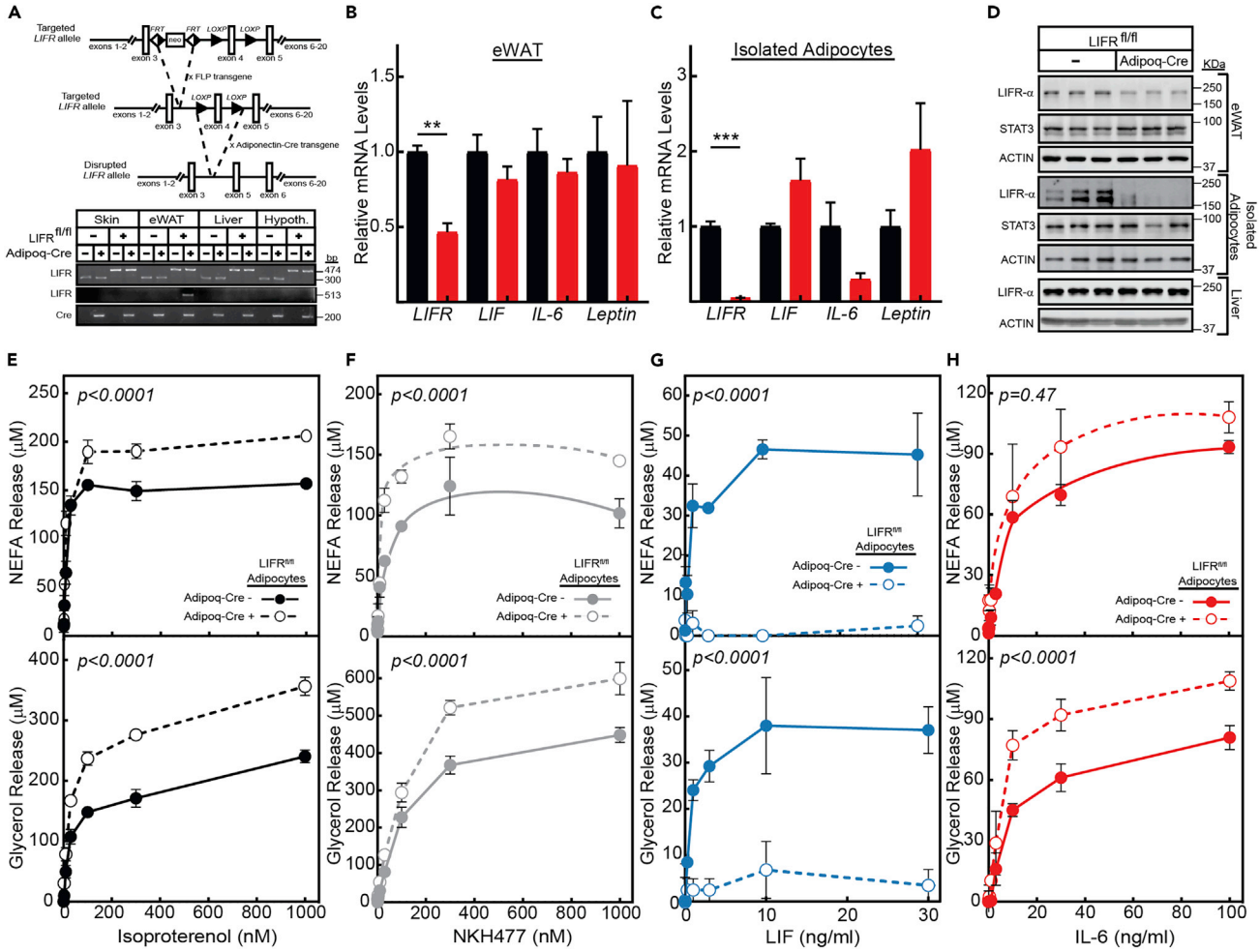

Figure 1. LIF-induced adipocyte inflammation and lipolysis require LIFR-α

(A) Schematic of the generation of *Adipoq-Cre;LIFR*$^{fl/fl}$ mouse model and genomic PCR of indicated tissue from male mice at 30 weeks of age from the indicated mouse model using primers for floxed *LIFR* allele (top panel), *LIFR* allele with deletion of exon 4 (middle panel), and *Cre* (bottom panel).

(B and C) qRT-PCR of eWAT (B) or isolated adipocytes from eWAT (C) from 4 *LIFR*$^{fl/fl}$ or *Adipoq-Cre;LIFR*$^{fl/fl}$ male mice at 30 weeks of age for the indicated gene normalized to β-actin. Data are shown as mean ± SEM.

(D) Immunoblot analysis of indicated tissue from three *LIFR*$^{fl/fl}$ or *Adipoq-Cre;LIFR*$^{fl/fl}$ male mice at 30 weeks of age with the indicated antibody.

(E–H) Differentiated adipocytes derived from *LIFR*$^{fl/fl}$ or *Adipoq-Cre;LIFR*$^{fl/fl}$ male mice at 7 weeks of age were treated with the indicated stimulants. After 20 h, medium non-esterified fatty acids (NEFA) and glycerol concentrations were measured (E–H). Data are shown as mean ± SEM. **p < 0.01 and ***p < 0.001 based on two-tailed *t* test with Bonferroni-Sidak adjustment for multiple comparison tests comparing *LIFR*$^{fl/fl}$ with *Adipoq-Cre;LIFR*$^{fl/fl}$ cohorts. p value calculated by using non-linear regression to fit a three-variable dose-response model to *LIFR*$^{fl/fl}$ to *Adipoq-Cre;LIFR*$^{fl/fl}$ cohorts, followed by an extra sum-of-squares *F* test for differences between cohort curves (E–H).

and *LIFR*$^{fl/fl}$-derived differentiated adipocytes (Figures 1E–1H). Although increasing concentrations of non-cytokines isoproterenol (Figure 1E) and NKH477 (Figure 1F) could still induce lipolysis, LIF (Figure 1G) was unable to stimulate lipolysis in *Adipoq-Cre;LIFR*$^{fl/fl}$ adipocytes. However, IL-6, which uses IL-6 receptor to transmit its inflammatory signal, was still able to induce lipolysis in the *Adipoq-Cre;LIFR*$^{fl/fl}$ adipocytes (Figure 1H). Although we observed increases in lipolysis of IL-6-treated *Adipoq-Cre;LIFR*$^{fl/fl}$ adipocytes compared with *LIFR*$^{fl/fl}$ adipocytes (Figure 1H), we also found the same proportional differences in the same adipocytes treated with non-cytokines (isoproterenol and NKH477) Figures 1E and 1F). We believe these increased levels of lipolysis arise from subtle differences in differentiation of this primary adipocyte cell line of this particular experiment. Successful generation of differentiated adipocytes derived from the *Adipoq-Cre;LIFR*$^{fl/fl}$ mouse model verified that LIF, but not IL-6 or non-cytokine stimulants, requires LIFR-α to induce adipocyte lipolysis.

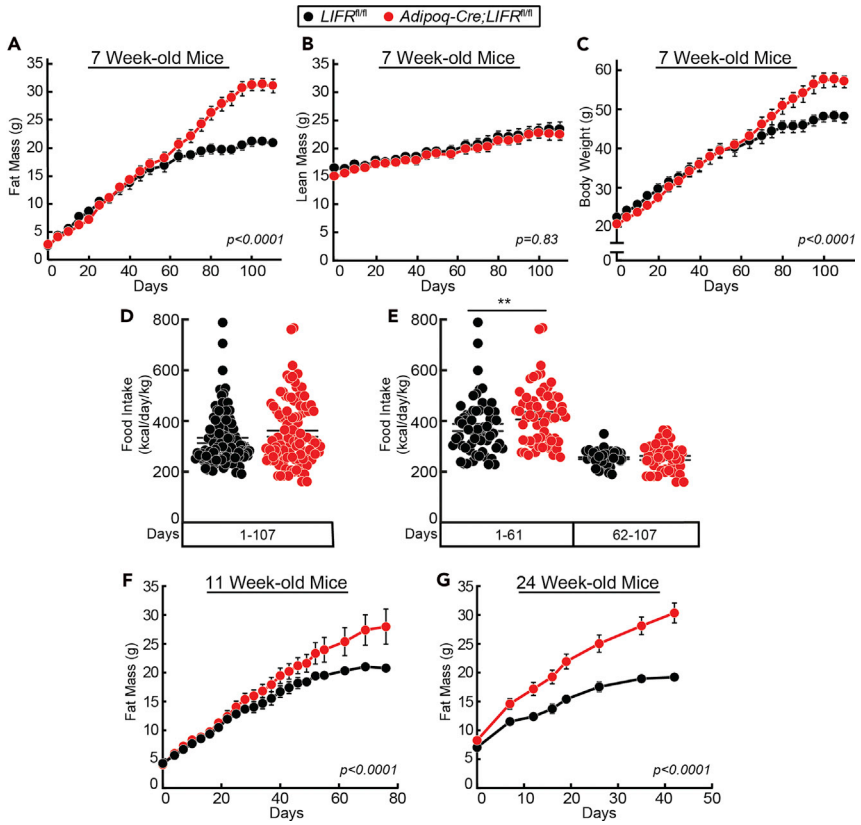

Figure 2. LIFR-α signaling in adipocytes suppresses adipose expansion in mice on a high fat diet

(A–G) *LIFR*$^{fl/fl}$ and *Adipoq-Cre;LIFR*$^{fl/fl}$ male mice at 7 weeks (A–E; n = 4), 11 weeks (F; n = 4), or 24 weeks (G; n = 5) of age were placed on a high-fat diet and fat mass by ECHO MRI (A, F, G), lean mass by ECHO MRI (B), body weight (C), and food intake (D and E) were measured over the indicated time period. Data are shown as mean ± SEM (A–C, F, and G) or dot plots with mean ± SEM (D–E). p was calculated using non-linear regression to fit a logistic growth curve to each cohort followed by extra sum-of-squares F test for significant differences between cohort curves (A–C, F, and G) or **p < 0.01 based on two-tailed t test (D) or a one-way ANOVA with Holm-Sidak's multiple comparison tests (E) comparing *LIFR*$^{fl/fl}$ with *Adipoq-Cre;LIFR*$^{fl/fl}$ cohorts.

See also Figure S1.

LIFR-α-induced adipocyte signaling suppresses adipose expansion and body weight gain in diet-induced obesity

Having established that LIFR-α regulates cytokine-mediated adipocyte lipolysis, we next studied how this signaling cascade affected mouse development. The *Adipoq-Cre;LIFR*$^{fl/fl}$ mice and littermate controls were produced at appropriate Mendelian frequencies with no obvious anatomic or physical differences. We subsequently evaluated the development of *Adipoq-Cre;LIFR*$^{fl/fl}$ mice and littermate controls at 5, 16, and 32 weeks of age. Body weights (Figure S1A), fat mass (Figures S1B and S1C), lean mass (Figures S1E and S1F), and food intake (Figure S1D) were not significantly different between each cohort at 5 and 16 weeks of age. At 32 weeks of age, the absolute fat mass of *Adipoq-Cre;LIFR*$^{fl/fl}$ mice was increased ~2-fold compared with controls (Figure S1B). This additional fat mass resulted in an ~20% increase in body weight at 32 weeks (Figure S1A). As a percentage of body weight, the knockout animals at 32 weeks of age had less contribution from lean mass (Figure S1F), a function of their increasing fat mass and its greater contribution to percentage body weight (Figure S1C).

To assess the role of LIFR-α adipose signaling in the setting of DIO, we placed *Adipoq-Cre;LIFR*$^{fl/fl}$ mice and littermate controls on an HFD (60% fat calories) at 7 weeks of age. Up to 62 days on HFD, there was no difference in fat mass between cohorts as determined by ECHO MRI (Figure 2A). Between 62 and 100 days, there was continued fat expansion in the *Adipoq-Cre;LIFR*$^{fl/fl}$ mice compared with controls that had a cessation of fat mass expansion resulting in a plateau. Only after 100 days did the *Adipoq-Cre;LIFR*$^{fl/fl}$ mice also

fail to demonstrate adipose expansion, leading to a plateau of absolute fat mass. At this point, the *Adipoq-Cre;LIFR*$^{fl/fl}$ mice had 50% more fat mass than *LIFR-α*$^{fl/fl}$ mice. There was no difference in ECHO MRI-measured lean mass throughout the experiment (Figure 2B). Body weight also diverged between 62 and 100 days on the HFD, coinciding with increasing differences in fat mass, with *Adipoq-Cre;LIFR*$^{fl/fl}$ mice weighing 33% more than littermate controls at the time of sacrifice (Figure 2C). When accounting for body weight, there was no difference in food intake between the *Adipoq-Cre;LIFR*$^{fl/fl}$ *and LIFR*$^{fl/fl}$ mice between days 62–107, the time frame during which there was a divergence in rates of fat expansion between these two models (Figure 2D and 2E).

Although there was a divergence in adipose mass between both models on HFD, we observed that it took approximately 60 days for the divergence to first initially manifest between the *Adipoq-Cre;LIFR*$^{fl/fl}$ *and LIFR*$^{fl/fl}$ mouse models. To determine if the age of the mice influenced the timing of the divergence in adipose mass between the *Adipoq-Cre;LIFR*$^{fl/fl}$ *and LIFR*$^{fl/fl}$ mouse model, we started both groups on an HFD at 11 (Figure 2F) and 24 weeks (Figure 2G) of age. Compared to the 7-week-old mice placed on an HFD with a starting fat mass of ~2.5 g (Figure 2A), the 11-week-old mice were placed on an HFD with a starting fat mass of ~5 g (Figure 2F) and the 24-week-old mice were placed on an HFD with a starting fat mass of ~7–8 g (Figure 2G). Our data showed that the divergence in fat mass between the *Adipoq-Cre;LIFR*$^{fl/fl}$ *and LIFR*$^{fl/fl}$ mouse models occurred at earlier time points for older compared to younger mouse cohorts placed on an HFD. Specifically, the divergence in fat mass occurred at ~60 days between the 7-week-old mice cohorts (Figure 2A), ~30 days between the 11-week-old mice cohorts (Figure 2F), and almost immediately between the 24-week-old mice cohorts (Figure 2G). Additionally, our studies showed that plateau in adipose mass of the *LIFR*$^{fl/fl}$ mouse models occurred between 15 and 20 g of fat mass and that of the *Adipoq-Cre;LIFR*$^{fl/fl}$ occurred between 25 and 30 g independent of the age at which HFD was initiated.

LIFR-α-induced adipocyte signaling limits adipose expansion in diet-induced obesity

As the *Adipoq-Cre;LIFR*$^{fl/fl}$ mice had greater capacity for adipose expansion on HFD compared with littermate controls, we next evaluated the white adipose tissue changes occurring over time in these mice. Consistent with the increased fat mass by ECHO MRI, the adipocytes appeared larger in the *Adipoq-Cre;-LIFR*$^{fl/fl}$ cohort compared with the littermate controls (Figures 3A and 3B). When quantifying adipocyte size, the *Adipoq-Cre;LIFR*$^{fl/fl}$ mice had on average 20% larger adipocyte diameters compared with littermate controls (Figure 3C). Specifically, the *Adipoq-Cre;LIFR*$^{fl/fl}$ mice had an average adipocyte diameter of 113 $\pm$ 2 μm compared with 89 $\pm$ 9 μm for adipocytes from littermate controls. Nearly 70% of the adipocytes from the *Adipoq-Cre;LIFR*$^{fl/fl}$ mice had diameters greater or equal to 101 μm compared with <40% for the *LIFR*$^{fl/fl}$ controls (Figure 3D). The histopathology analysis of eWAT correlated with the fat expansion measured with ECHO MRI in the *Adipoq-Cre;LIFR*$^{fl/fl}$ mice fed an HFD.

We next assessed gene expression changes in the eWAT of *LIFR* knockout mice and littermate controls fed an HFD. At the end of the experiment, when there was no further adipose expansion leading to a plateau of adipose mass in both groups (day 107), mRNA expression of *IL6* and *SOCS3,* both target genes of STAT3, were increased ~2-fold compared with littermate controls (Figure 3E). Furthermore, *LIFR* mRNA expression levels were no longer significantly different than controls. This is in contrast to the decreased *LIFR* and *IL-6* expression identified in the adipocytes of eWAT from the *Adipoq-Cre;LIFR*$^{fl/fl}$ mice on a regular chow diet compared with littermate controls (see Figure 1D). Knowing that LIF and other IL-6 family cytokines are activators of adipocyte lipolysis, we next evaluated mRNA expression of genes critical to TAG synthesis or lipolysis in adipose tissue in these models. Although there was a trend toward decreased mRNA expression of several re-esterification enzymes, there were no significant differences in the expression of genes involved in adipocyte TAG synthesis or lipolysis between cohorts (Figures 3F and 3G). Figure 3H shows that genetic disruption of *LIFR* in adipocytes suppressed induction of multiple browning markers, including the genes encoding UCP1 and PGC-1α (*ppargc1a). UCP1* expression was decreased in inguinal, subcutaneous, and epididymal, but not brown adipose tissue in *Adipoq-Cre;LIFR*$^{fl/fl}$ mice on an HFD compared with littermate controls (Figure 3I).

To measure the contribution of adipocyte LIFR-α activation of STAT3 in adipose tissue, we subjected eWAT from *Adipoq-Cre;LIFR*$^{fl/fl}$ and *LIFR*$^{fl/fl}$ mice fed an HFD to immunoblot analysis of phosphorylated STAT3 and H&E evaluation at multiple time points. Preceding a divergence in adipose expansion and absolute fat mass (day 21), the adipose from the littermate controls had increased STAT3 phosphorylation compared

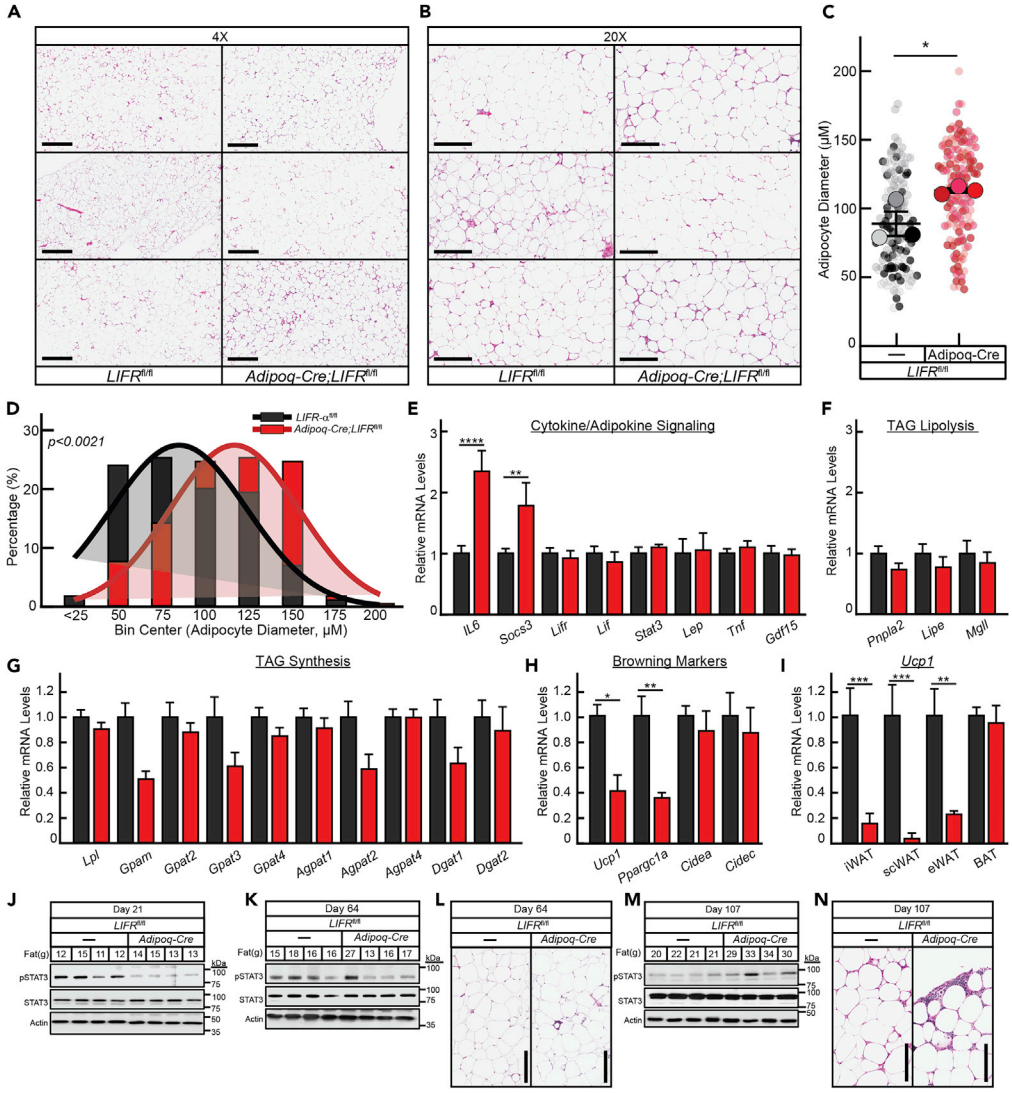

Figure 3. Adipocyte LIFR-α signaling activates STAT3-suppressing adipose expansion in mice on a high-fat diet

(A–D) *LIFR*$^{fl/fl}$ and *Adipoq-Cre;LIFR*$^{fl/fl}$ male mice (n = 4) at 7 weeks of age were placed on an HFD as described in Figure 2. Mice were sacrificed, and eWAT was harvested and processed for H&E histopathology with subsequent measurement of adipocyte diameters from 3 mice per cohort (C and D). Data are shown as dot plots with mean ± SEM (C). *p < 0.05 based on one-tailed Student's t test (C) or p was calculated using non-linear regression to fit a Gaussian curve to each cohort followed by extra sum-of-squares F test for significant differences between cohort curves (D). Scale bars: 600 μm in (A) and 300 μm in (B).

(E–I) qRT-PCR of the indicated genes normalized to β-actin from two experiments containing 8 total mice per cohort in which *LIFR*$^{fl/fl}$ and *Adipoq-Cre;LIFR*$^{fl/fl}$ male mice at 7 and 10 weeks of age were sacrificed after 107 and 72 days, respectively, on an HFD. Data are shown as mean ± SEM. *p < 0.05, **p < 0.01, ***p < 0.001, and ****p < 0.0001 based on a two-way ANOVA with Fischer's LSD multiple comparison tests comparing *LIFR*$^{fl/fl}$ and *Adipoq-Cre;LIFR*$^{fl/fl}$ cohorts.

(J–N) *LIFR*$^{fl/fl}$ and *Adipoq-Cre;LIFR*$^{fl/fl}$ male mice at 7 weeks of age placed on an HFD were sacrificed at 21 (J), 64 (K and L), or 107 days (M and N), and eWAT was processed for immunoblot analysis with the indicated antibodies (21 (J), 64 (K), or 107 days (J and K, M)) or H&E histopathology as described in transparent methods. Scale bar, 200 μm in (L and N).

See also Figure S2.

with the *Adipoq-Cre;LIFR*$^{fl/fl}$ mice (Figure 3J), consistent with the lack of LIFR-α signaling in the adipocyte. At the time of initial divergence in fat expansion and mass (day 64), the littermate controls demonstrated persistent STAT3 phosphorylation (Figure 3K). A majority of the knockout mice had decreased STAT3 phosphorylation compared with littermate controls. At the time that all *Adipoq-Cre;LIFR*$^{fl/fl}$ mice had reached a plateau of 50% more fat mass and no further expansion (day 107), the eWAT from the *Adipoq-Cre;LIFR*$^{fl/fl}$

mice now demonstrated more STAT3 phosphorylation than littermate controls (Figure 3M). This increase in STAT3 phosphorylation of eWAT at later time points correlated with increased patchy lymphocyte infiltration into the eWAT of *Adipoq-Cre;LIFR*$^{fl/fl}$ mice compared with littermate controls by H&E evaluation (Figure 3N). As further corroboration, we observed an ~2-fold average increase in crown-like structures in the eWAT of *Adipoq-Cre;LIFR*$^{fl/fl}$ mice (11.25 average crown-like structures per 20 HPF) compared with the *LIFR*$^{fl/fl}$ mice littermate controls (5.6 average crown-like structures per 20 HPF) at the later time points. This infiltration of lymphocytes in eWAT of *Adipoq-Cre;LIFR*$^{fl/fl}$ mice (Figure 3L) and differences in average crown-like structures between cohorts was not observed at the earlier time points. Overall, mice with an intact LIFR-α inflammatory signaling axis had earlier STAT3 activation compared with *Adipoq-Cre;LIFR*$^{fl/fl}$ mice, which was associated with reduced adipose expansion/adipocyte diameter and increased browning markers. Once the *Adipoq-Cre;LIFR*$^{fl/fl}$ mice reached a 50% increase in adipose mass, they had increased lymphocyte infiltration in eWAT, which ultimately associated with increased STAT3 phosphorylation. Finally, we assessed if levels of serum markers of adipocyte lipolysis (glycerol, NEFA, and triacylglycerides) were different between *LIFR*$^{fl/fl}$ and *Adipoq-Cre;LIFR*$^{fl/fl}$ mice (Figure S2A–S2C). In longitudinal evaluations of serum after fasting, there was no significant difference in these markers between these cohorts.

LIFR-α-induced adipocyte signaling promotes hepatic triacylglyceride accumulation

In demonstrating that *Adipoq-Cre;LIFR*$^{fl/fl}$ mice reached significantly higher levels of adipose expansion than *LIFR*$^{fl/fl}$ littermate controls on an HFD by gross inspection, histology, and ECHO MRI quantification, we also observed that the *LIFR*$^{fl/fl}$ animals had livers that were larger and paler than their *Adipoq-Cre;-LIFR*$^{fl/fl}$ counterparts on gross evaluation (Figures 4A and 4B). Histopathological analysis of H&E sections of livers of from *LIFR*$^{fl/fl}$ mice demonstrated increased microvesicular and macrovesicular steatosis compared with H&E sections of livers from *Adipoq-Cre;LIFR*$^{fl/fl}$ mice (Figures 4C and 4D). We next assessed for associations between liver lipid levels and size relative to body weight or fat mass over multiple cohorts and experiments sacrificed at different time points during the divergence of adipose expansion between the two models on HFD. The control *LIFR*$^{fl/fl}$ mice showed a peak in liver TAGs once they reached ~45 g or greater in body weight (Figure 4F) or 18 g or greater of fat mass (Figure 4I). This level of body weight and adipose mass coincided with the point of no further adipose expansion, resulting in the plateau of adipose mass in the control mouse cohort (see Figures 2A and 2C). At the body weight (~45 g) and adipose mass (~18 g) at which littermate controls demonstrated maximal liver TAG levels, the *Adipoq-Cre;LIFR*$^{fl/fl}$ mice consistently had lower liver TAG levels (Figures 4E and 4H). The *Adipoq-Cre;LIFR*$^{fl/fl}$ mice finally demonstrated similar levels of liver TAGs to the littermate controls only after gaining an additional 50% increase in adipose mass (greater than 28 g) and ~20% in body weight (greater than 55 g), which coincided with no further adipose expansion and plateau in their adipose mass. Similar differences between *Adipoq-Cre;-LIFR*$^{fl/fl}$ mice and littermate controls were observed when comparing liver mass to body weight (Figure 4E) or fat mass (Figure 4H). There were no significant differences between these models with respect to the association of liver cholesterol to body weight (Figure 4G) or fat mass (Figure 4J). Overall, disrupting the adipocyte LIFR-α inflammatory signaling axis in mice on an HFD not only allowed for a 50% increase in adipose expansion but also led to a net reduction in ectopic liver TAG accumulation and a lower liver mass. Only after the *Adipoq-Cre;LIFR*$^{fl/fl}$ model reached a plateau of adipose mass (50% increase compared with controls) was the ectopic liver TAG accumulation and mass comparable to littermate controls.

Effects of adipocyte LIFR-α signaling on insulin responsiveness and respiration in diet-induced obesity

Insulin resistance contributes to NAFLD through hepatic intrinsic and extrinsic signaling events (Samuel and Shulman, 2018; Utzschneider and Kahn, 2006). In the adipocyte, insulin resistance leads to decreased insulin-mediated suppression of TAG lipolysis, thereby supplying more glycerol and fatty acids to the liver, contributing to NAFLD (Shulman, 2000; Titchenell et al., 2017). Having demonstrated the importance of adipocyte LIFR-α inflammatory signaling in DIO to increasing lipolysis limiting adipose expansion and leading to ectopic liver TAG accumulation, we next assessed if signaling through this axis influenced insulin responsiveness leading to NAFLD. *Adipoq-Cre;LIFR*$^{fl/fl}$ and *LIFR*$^{fl/fl}$ mice on an HFD were evaluated with glucose and insulin tolerance tests at baseline, at the point of divergence of fat mass (day 55; adipose mass ~18 g), and after both models had reached their plateau in adipose mass (day 140; *Adipoq-Cre;-LIFR*$^{fl/fl}$ fat mass ~28 g, *LIFR*$^{fl/fl}$ fat mass ~18 g). Figures 5A and 5B demonstrated no statistical differences in glucose or insulin tolerance at any of these points, even though knockout mice had 50% more adipose and body weight than littermate controls at greater than 140 days. Despite having similar insulin

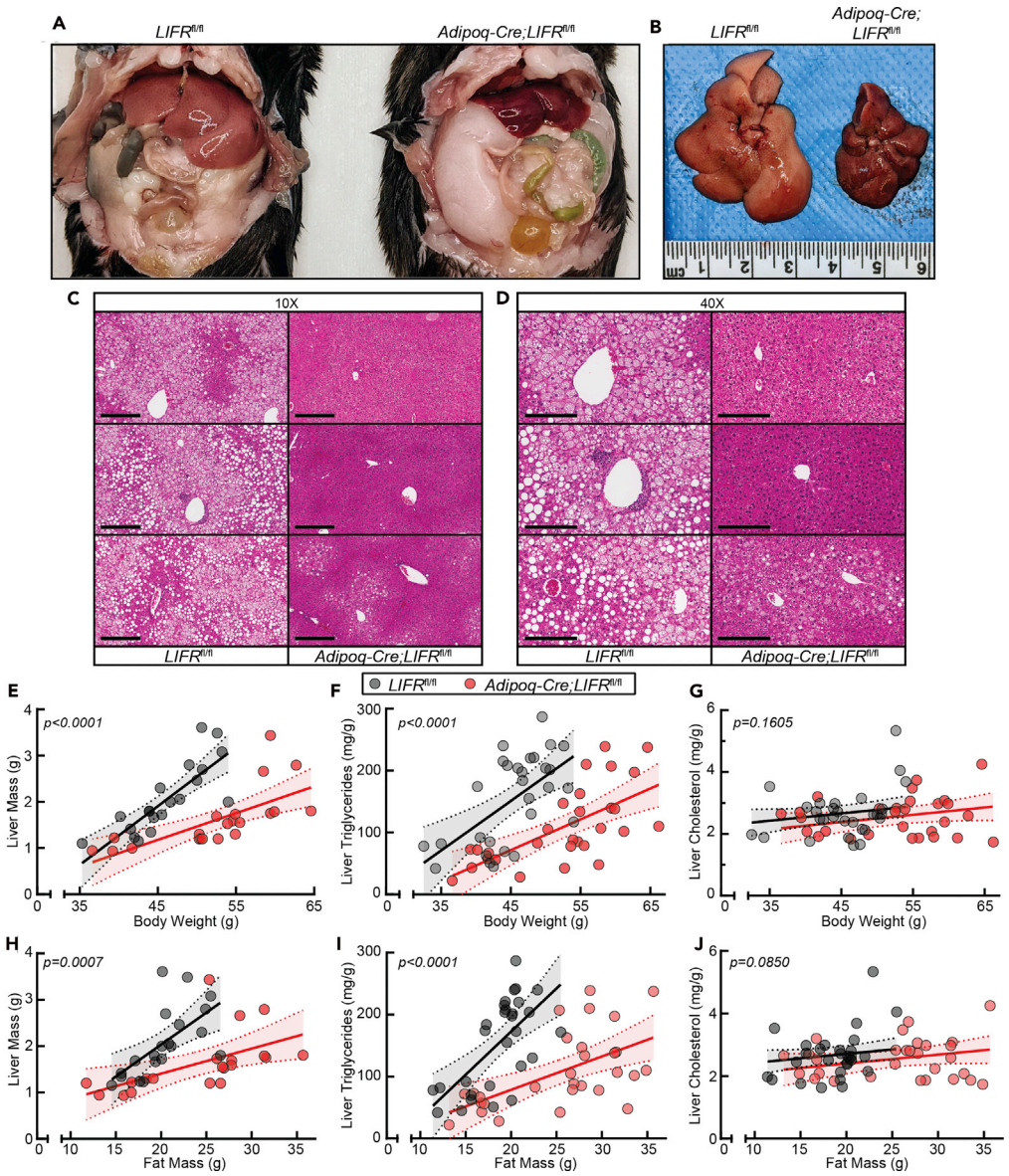

Figure 4. LIFR-α-induced adipocyte signaling promotes hepatic triacylglyceride accumulation in mice on a high-fat diet

(A–J) Representative gross (A and B) and H&E histopathology images of liver from representative *LIFR*$^{fl/fl}$ and *Adipoq-Cre;LIFR*$^{fl/fl}$ male mice on an HFD at sacrifice (day 107) from Figures 2. (E–J) Age-matched *LIFR*$^{fl/fl}$ and *Adipoq-Cre;LIFR*$^{fl/fl}$ male mice at age 7 (n = 4), 7 (n = 4), 8 (n = 8), 10 (n = 4), 12 (n = 4), 22 (n = 3), or 25 (n = 5) weeks were placed on an HFD and sacrificed after 110, 21, 144, 75, 63, 58, or 42 days, respectively. Body weight, fat mass by ECHO MRI, liver mass, liver TAGs, and liver cholesterol were measured at sacrifice. Linear regression analysis was conducted to determine the association of liver mass (E and H), TAGs (F and I), and cholesterol (G and J) to body weight (E–G) or fat mass (H–J). Data are shown as dot plots with regression line and 95% confidence band. p was calculated using extra sum-of-squares *F* test for significant differences between regression lines for *LIFR*$^{fl/fl}$ and *Adipoq-Cre;LIFR*$^{fl/fl}$ cohorts (E–J). Scale bars: 300 μm in (C) and 200 μm in (D).

responsiveness, the *Adipoq-Cre;LIFR*$^{fl/fl}$ mice had decreased NAFLD, suggesting that insulin responsiveness is not the sole contributor to NAFLD development in the HFD mouse model.

Considering there was a difference in mRNA expression of browning markers in multiple depots of adipose tissue between *Adipoq-Cre;LIFR*$^{-fl/fl}$ and *LIFR*$^{fl/fl}$ mice on an HFD, we next housed individual mice in

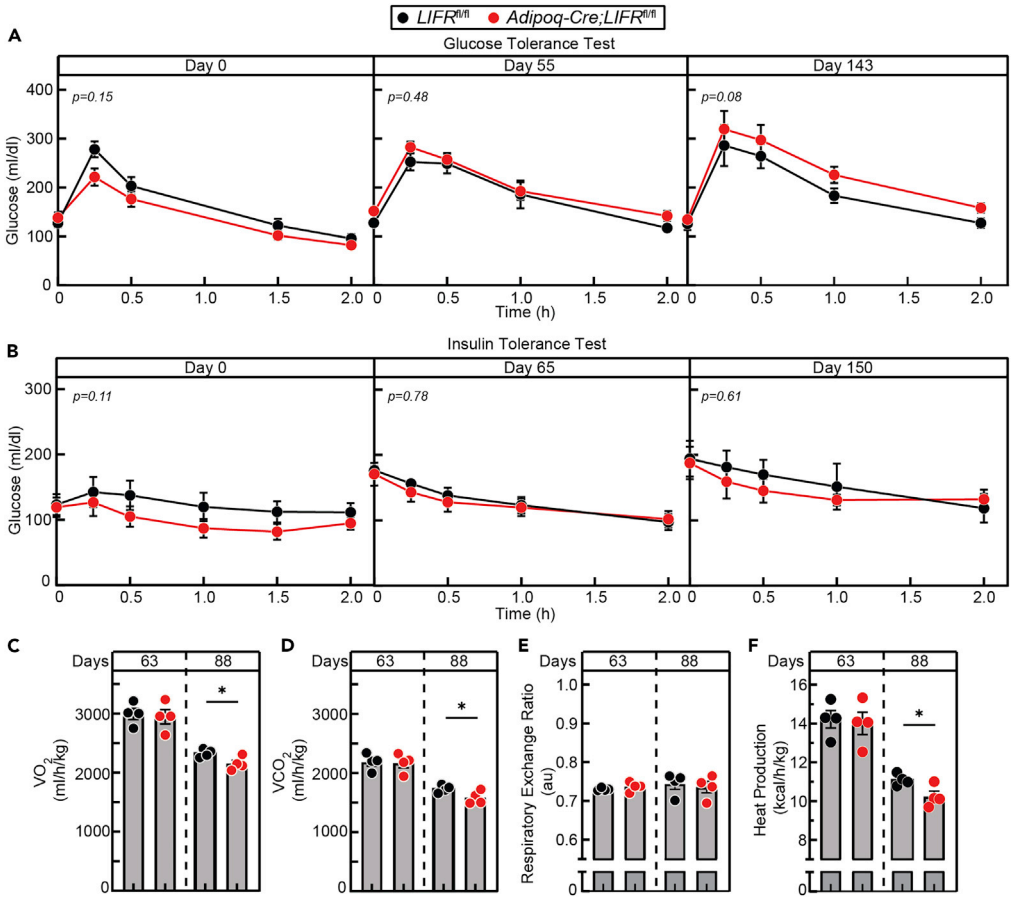

Figure 5. Insulin responsiveness and respiration of *Adipoq-Cre;LIFR*$^{fl/fl}$ mice on a high-fat diet

(A and B) *LIFR*$^{fl/fl}$ and *Adipoq-Cre;LIFR*$^{fl/fl}$ male mice (n = 4) at 7 weeks of age were placed on an HFD. Glucose tolerance test (A) and insulin tolerance test (B) were performed on animals at the indicated time point as described in transparent methods. Data are shown as mean ± SEM. p calculated by two-tailed unpaired Student's t test for significant differences between the area under curve (baseline 0 mg/dL) for each group.

(C–F) LIFR$^{fl/fl}$ and Adipoq-Cre; LIFR$^{fl/fl}$ male mice at 10 weeks of age were placed on a high-fat diet followed by metabolic measurement with CLAMS as described in transparent methods at the indicated time points. Data are shown as dot plots with mean ± SEM. *p < 0.05 based on two-way ANOVA with Sidak's multiple comparison tests comparing *LIFR*$^{fl/fl}$ and *Adipoq-Cre;LIFR*$^{fl/fl}$ cohorts.

metabolic cages at each of the following times: (1) at the point of fat mass divergence and (2) after both cohorts had reached a plateau in fat mass. Before any differences in body weight or adipose mass on an HFD, there were no differences in VO_2 (Figure 5C, left panel), VCO_2 (Figure 5D, left panel), respiratory exchange ratio (Figure 5E, left panel), and heat production (Figure 5F, left panel) between genetic models. Once the *Adipoq-Cre;LIFR*$^{fl/fl}$ mice gained more body weight and adipose mass on an HFD than *LIFR*$^{fl/fl}$ mice, they displayed lower VO_2 (Figure 5C, right panel) and VCO_2 (Figure 5D, *right panel*) at similar proportions resulting in no difference in respiratory exchange ratio (Figure 5E, right panel). The *Adipoq-Cre;LIFR*$^{fl/fl}$ mice also had a significant reduction in heat production when accounting for body weight changes between the groups (Figure 5F, right panel).

STAT3 is required for LIF- and IL-6-mediated adipocyte lipolysis

We have now shown that LIF signals through its receptor LIFR-α to induce STAT3 activation and adipocyte lipolysis in adipose. We previously showed that LIF and other IL-6 family members increase the lipolysis potential of the adipocyte through a JAK-dependent mechanism (Arora et al., 2020). Although we observed an association of STAT3 phosphorylation with LIF and IL-6-mediated lipolysis, there was no evidence that STAT3 was required for IL-6 family cytokine-mediated adipocyte lipolysis. Therefore, we created an

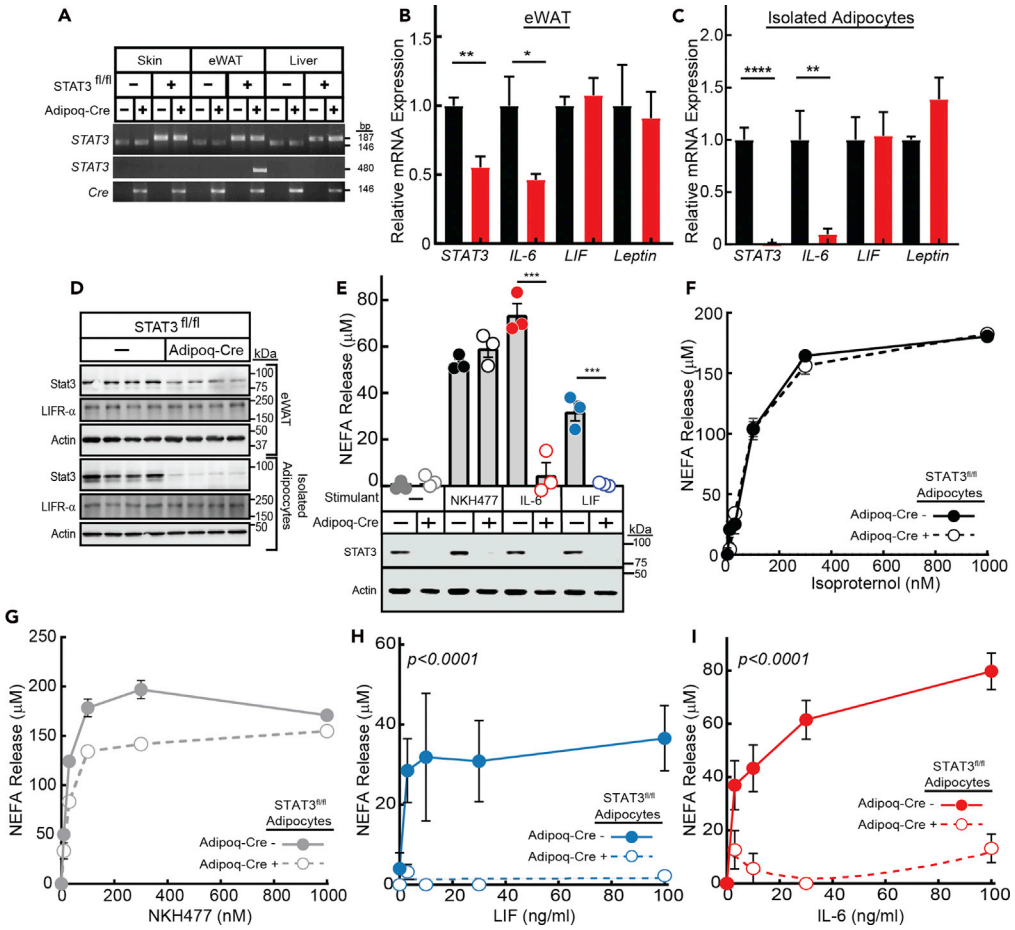

Figure 6. LIF- and IL-6-induced adipocyte lipolysis signaling requires STAT3

(A) Genomic PCR of indicated tissue from male mice at 30 weeks of age from the indicated mouse model using primers for floxed *STAT3* allele (top panel), *STAT3* allele with deletion of exons 18–20 (middle panel), and *Cre* (bottom panel).

(B and C) qRT-PCR of eWAT (B) or isolated adipocytes from eWAT (C) from four *STAT3*$^{fl/fl}$ or *Adipoq-Cre;STAT3*$^{fl/fl}$ male mice at 30 weeks of age for the indicated gene normalized to β-actin. Data are shown as mean ± SEM. *p<0.05, **p<0.01, and ****p<0.0001 based on two-tailed Student's t test with Bonferroni-Sidak adjustment for multiple comparison tests

(D) Immunoblot analysis of whole tissue or adipocytes isolated from eWAT from four *STAT3*$^{fl/fl}$ or *Adipoq-Cre;STAT3*$^{fl/fl}$ male mice at 30 weeks of age with the indicated antibody as described.

(E–I) Differentiated adipocytes derived from *STAT3*$^{fl/fl}$ or *Adipoq-Cre;STAT3*$^{fl/fl}$ male mice at 7 weeks of age were treated with the indicated stimulants. After 20 h, cells were processed for immunoblot analysis (E) and medium NEFA concentrations were measured. Data are shown as dot plots with mean ± SEM (E) or as as mean ± SEM (F-I). ***p < 0.001 based on two-way ANOVA with Sidak's adjustment for multiple comparison tests comparing *STAT3*$^{fl/fl}$ with *Adipoq-Cre;STAT3*$^{fl/fl}$ cohorts (E) or p value calculated by using non-linear regression to fit a three-variable dose-response model to *STAT3*$^{fl/fl}$ to *Adipoq-Cre;STAT3*$^{fl/fl}$ cohorts, followed by an extra sum-of-squares *F* test for differences between cohort curves (F–I).

Adipoq-Cre;STAT3$^{fl/fl}$ mouse model to determine if STAT3 is necessary for LIF- and IL-6-induced adipocyte inflammatory signaling supporting lipolysis as described in transparent methods. The *Adipoq-Cre;STAT3*$^{fl/fl}$ mice and *STAT3*$^{fl/fl}$ littermate controls were produced at appropriate Mendelian frequencies with no obvious anatomic or physical differences, including in the development of adipose. We conducted PCR of genomic DNA obtained from skin, eWAT, and liver to verify that *STAT3* was only disrupted in white adipose tissue (Figure 6A). In Figure 6B, *STAT3* and *IL6* mRNA expression levels were decreased by approximately 50% in the *Adipoq-Cre;STAT3*$^{fl/fl}$ mice compared with *STAT3*$^{fl/fl}$ littermate controls in eWAT. Differentiated adipocytes derived from WAT demonstrated a complete suppression of *STAT3* and significantly reduced expression of *IL6* mRNA (Figure 6C). Immunoblot analysis showed reduced STAT3 protein levels in the eWAT of knockout mice, further reduced to near-absent levels in the isolated adipocyte fractions of this

tissue compared with littermate controls (Figure 6D). LIFR-α remained unchanged between knockout and littermate controls in eWAT and isolated adipocyte fractions, verifying that genetic disruption of *STAT3* expression did not affect the protein level of LIFR-α.

To assess if STAT3 is critical for transducing LIF- and IL-6-mediated signaling that increases the adipocyte lipolysis potential, we differentiated adipocytes from the SVFs of *Adipoq-Cre;STAT3*$^{fl/fl}$ mice and littermate controls and conducted lipolysis assays in the absence or presence of isoproterenol, NKH477, IL-6, and LIF. The absence of STAT3 in *Adipoq-Cre;STAT3*$^{fl/fl}$-derived adipocytes completely suppressed LIF- (Figures 6E and 6H) and IL-6- (Figures 6E and 6I) induced lipolysis as judged by NEFA release from adipocytes into the medium, but had no significant effect on the non-cytokines isoproterenol (Figure 6F) and NKH477 (Figure 6G). These findings establish that STAT3 is required for LIF- and IL-6-mediated adipocyte lipolysis signaling.

STAT3-dependent adipocyte signaling limits adipose expansion and body weight gain

LIFR-α-dependent adipocyte signaling in DIO promoted lipolysis suppressing adipose expansion, leading to the development of NAFLD. We also showed that LIFR-α-dependent adipocyte lipolysis signaling required STAT3. Therefore, we placed the *Adipoq-Cre;STAT3*$^{fl/fl}$ mouse model on an HFD to determine if the changes to fat mass, body weight, and ectopic liver TAG accumulation matched that of the adipocyte-specific *LIFR* knockout. Phenotypic adaptations of the *Adipoq-Cre;STAT3*$^{fl/fl}$ model to an HFD (Figures 7A–7C) matched the adaptations of the *Adipoq-Cre;LIFR*$^{fl/fl}$ model on an HFD (see Figures 2A–2C) with respect to fat expansion, absolute fat mass, lean mass, and body weight when compared with littermate controls. Up to ~65 days on HFD, there was no difference in fat mass between cohorts as determined by ECHO MRI (Figure 7A). After ~65 days (starting at ~16–18 g of fat mass), the levels of adipose mass began separating between the *Adipoq-Cre;STAT3*$^{fl/fl}$ mice and littermate controls on an HFD. After 110 days, the *Adipoq-Cre;STAT3*$^{fl/fl}$ mice had a reduced rate of fat expansion also resulting in a plateau of fat mass. At this point, the *Adipoq-Cre;STAT3*$^{fl/fl}$ mice had 50% more fat mass (~28 g) compared with the *STAT3*$^{fl/fl}$ mice (~18–20 g), similar to the adipose mass findings in the *Adipoq-Cre;LIFR*$^{fl/fl}$ model on an HFD (see Figure 2A). The *Adipoq-Cre;STAT3*$^{fl/fl}$ mice model on an HFD showed no difference in ECHO MRI-measured lean mass compared with littermate controls (Figure 7B), similar to the lean mass findings in the *Adipoq-Cre;LIFR*$^{fl/fl}$ model on an HFD (see Figure 2B). Body weight also diverged between 65 and 110 days on the HFD coinciding with fat mass differences, with *Adipoq-Cre;STAT3*$^{fl/fl}$ mice weighing ~30% more than littermate controls at the time of sacrifice (Figure 7C), similar to the body weight differences observed in the *Adipoq-Cre;LIFR*$^{fl/fl}$ model on an HFD (see Figure 2C). Finally, we assessed if levels of serum markers of adipocyte lipolysis (glycerol, NEFA, and triacylglycerides) were different between *STAT3*$^{fl/fl}$ and *Adipoq-Cre;STAT3*$^{fl/fl}$ mice (Figures S2D–S2F). Evaluation of serum in the non-fasting and fasting state demonstrated no significant differences in these markers between these cohorts.

Overall, the congruence in the phenotypes of the *Adipoq-Cre;LIFR*$^{fl/fl}$ and *Adipoq-Cre;STAT3*$^{fl/fl}$ mouse models suggests that LIFR-α-dependent inflammatory signaling uses STAT3 to transmit its suppressive actions for fat expansion in DIO. After reaching a 50% increase in fat mass compared with controls, both the *Adipoq-Cre;STAT3*$^{fl/fl}$ and *Adipoq-Cre;LIFR*$^{fl/fl}$ mouse models reached a limit in fat expansion causing a plateau in body weight and fat mass. These data suggest that the eventual decrease in fat expansion in the *Adipoq-Cre;LIFR*$^{fl/fl}$ mouse model is not an adipocyte STAT3-dependent process.

STAT3-induced adipocyte inflammation promotes hepatic triacylglyceride accumulation

There have been two other studies that previously silenced *STAT3* in adipose tissue, and both these studies also demonstrated an increase in fat mass and body weight in mice fed a regular chow diet or an HFD (Cernkovich et al., 2008; Reilly et al., 2020). The latter study characterized catecholamine-driven adipocyte STAT3-dependent reprogramming of adipocytes in an HFD. However, they did not evaluate this *Adipoq-Cre;STAT3*$^{fl/fl}$ model for its effect on adipose inflammation and its role in adipocyte lipolysis in DIO. Interestingly, they did not identify any differences in ectopic liver TAG accumulation between *Adipoq-Cre;STAT3*$^{fl/fl}$ mice and littermate controls as seen in our *Adipoq-Cre;LIFR*$^{fl/fl}$ model. There are two possible explanations for this discrepancy: (1) their assessment of liver TAGs was conducted at a point where the fat mass and body weight had already plateaued in the *Adipoq-Cre;STAT3*$^{fl/fl}$ mice increasing ectopic liver TAGs or (2) the LIFR-α inflammation-induced NAFLD observed during DIO is due to a STAT3-independent pathway such as YAP/Hippo (Tamm et al., 2011).

To determine if LIFR-α-dependent adipocyte signaling requires STAT3 to promote ectopic hepatic TAG accumulation, we assessed NAFLD development in the *Adipoq-Cre;STAT3*$^{fl/fl}$ mice on an HFD. We

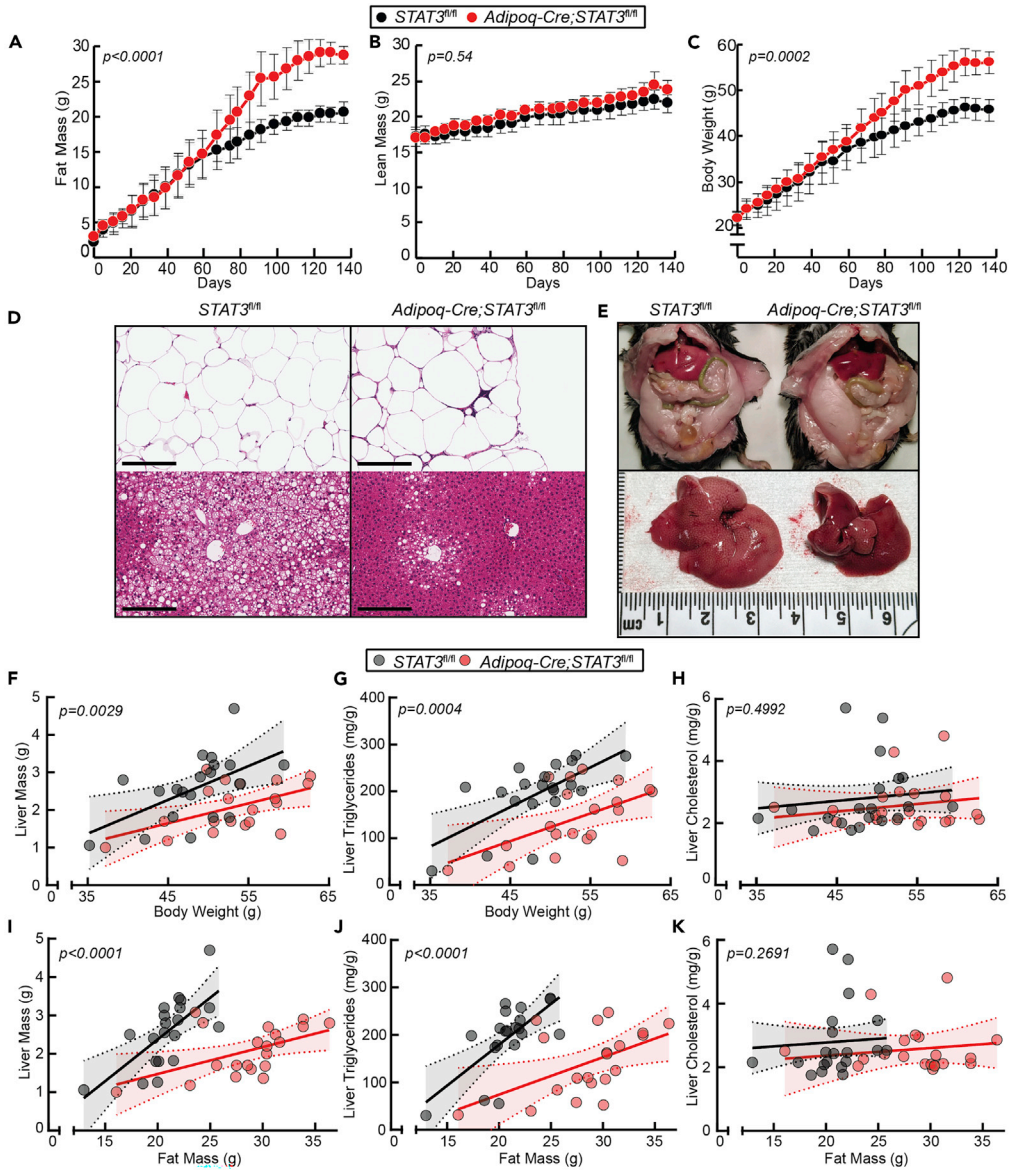

Figure 7. STAT3-dependent adipocyte signaling limits adipose expansion promoting hepatic triacylglyceride accumulation

(A–D) *STAT3*$^{fl/fl}$ and *Adipoq-Cre;STAT3*$^{fl/fl}$ male mice (n = 4) at 8 weeks of age were placed on HFD and fat mass by ECHO MRI (A), lean mass by ECHO MRI (B), and body weight (C) were measured over the indicated time period. Mice were sacrificed, tissues were harvested, and representative H&E images of eWAT and liver were obtained (D, scale bar, 200 μm). Data are shown as mean ± SEM (A-C). p was calculated using non-linear regression to fit a logistic growth curve to each cohort followed by extra sum-of-squares F test for significant differences between cohort curves (A–C).

(E) Representative gross whole-body and liver images of *STAT3*$^{fl/fl}$ and *Adipoq-Cre;STAT3*$^{fl/fl}$ male mice at 20 weeks of age after being on an HFD for 84 days.

(F–K) *STAT3*$^{fl/fl}$ and *Adipoq-Cre;STAT3*$^{fl/fl}$ male mice at 7 (n = 3), 7 (n = 3), 8 (n = 6), 8 (n = 4), and 32 (n = 4) weeks of age were placed on an HFD and sacrificed after 93, 126, 84, 136, and 95 days, respectively. Body weight, fat mass by ECHO MRI, liver mass, liver TAGs, and liver cholesterol were measured at sacrifice. Linear regression analysis was conducted to determine the association of liver mass (F and I), TAGs (G and J), and cholesterol (H and K) to body weight (F–H) or fat mass (I–K). Data are shown as scattered plots with regression line and 95% confidence band. p was calculated using sum-of-squares *F* test for significant differences between linear regression curves (F–K).

See also Figure S2.

consistently observed that the *STAT3*$^{fl/fl}$ animals had livers that were larger and paler compared with their *Adipoq-Cre;STAT3*$^{fl/fl}$ counterparts on gross evaluation (Figure 7E). H&E analysis of the liver demonstrated increased microvesicular and macrovesicular steatosis in the *STAT3*$^{fl/fl}$ mice compared with the *Adipoq-Cre;STAT3*$^{fl/fl}$ mice (Figure 7D, bottom images). On analysis of H&E sections of eWAT, *STAT3*$^{fl/fl}$ mice had decreased adipocyte size (Figure 7D, upper images) and an ~2-fold decrease in crown-like structures (9 average crown-like structures per 20 high-power fileds) compared with *Adipoq-Cre;STAT3*$^{fl/fl}$ mice (18 average crown-like structures per 20 high-power fileds). To further assess if LIFR-α signaling-induced NAFLD is dependent or independent of STAT3, we performed regression analysis to evaluate liver TAGs at different body weights and fat masses in the *Adipoq-Cre;STAT3*$^{fl/fl}$ mouse model. The control *STAT3*$^{fl/fl}$ mice showed elevated liver TAGs once they reached ~45 g body weight (Figure 7G) or ~18–20 g of fat mass (Figure 7J). This level of body weight and fat mass coincided with the point of no further adipose expansion resulting in the plateau of body weight and adipose mass in the control mice cohort (see Figures 7A and 7C). At ~45 g of body weight and ~18–20 g of adipose mass, *Adipoq-Cre;STAT3*$^{fl/fl}$ mice consistently had lower liver TAG levels than their littermate controls. The *Adipoq-Cre;STAT3*$^{fl/fl}$ mice only consistently reached similar levels of increased TAGs to their wild-type counterparts only after having further fat mass expansion leading to greater than ~28 g of adipose mass and greater than ~55 g of body weight, which coincided with no further fat expansion and plateau in their fat mass. The differences in liver TAGs as a function of body weight and fat mass found between genetic models were also found with liver mass (Figures 7F and 7I). There were no significant differences of hepatic cholesterol in relation to body weight (Figure 7H) or fat mass (Figure 7K) within and between genetic models. These significant differences in ectopic liver TAGs and liver size observed in the *Adipoq-Cre;STAT3*$^{fl/fl}$ mice compared with littermate controls are similar to those found in the *Adipoq-Cre;LIFR*$^{fl/fl}$ mouse model (see Figures 4E–4J). Overall, these data support STAT3 dependence of LIFR-α adipocyte signaling in the development of NAFLD in DIO.

DISCUSSION

Although obesity is associated with adipose inflammation, the role of cytokine inflammatory signaling in regulating adipose expansion and related metabolic sequelae remain unclear. Previously, we provided insight into how IL-6 family cytokines, including LIF, induce adipose inflammation and lipolysis in a JAK-dependent manner to regulate adipose levels in mouse models of obesity and cachexia (Arora et al., 2018, 2020). In this study, we addressed the role of LIFR-α adipocyte signaling during DIO-associated metabolic states of adipose inflammation. With differentiated adipocytes generated from an adipocyte-specific *LIFR* knockout mouse model, we showed that LIF requires LIFR-α to induce STAT3 activation and adipocyte lipolysis. Consistent with (1) increased LIF protein in serum and adipose in preclinical obesity mouse models and obese patients and (2) reduced inflammation-associated lipolysis potential in *LIFR*-disrupted adipocytes, the adipocyte-specific *LIFR* knockout mouse model on an HFD displayed decreased markers of adipose inflammation and browning that was associated with a 50% increase in adipocyte/adipose expansion and 20% increase in body weight. Despite a significant increase in adipose mass and body weight, these adipocyte-specific *LIFR* knockout mice had a significant decrease in steatosis development without any significant differences in glucose responsiveness and insulin tolerance. Finally, at time points of equivalent adipose mass and body weight, the adipocyte-specific *LIFR* knockout mice had greater than 2-fold reduction in TAG concentration and greater than 2-fold decrease in liver mass, resulting in ~75% reduction in total liver TAGs compared with littermate controls. The adipocyte-specific *STAT3* knockout mouse model had a similar phenotype to the adipocyte-specific *LIFR* knockout mouse model on an HFD—decreased cytokine-induced lipolysis, increased adipose expansion, and decreased NAFLD. Combined, these data suggest that LIFR-α/JAK/STAT3 adipocyte inflammatory signaling directly contributes to the development of increased lipolysis potential and browning, suppressing adipose expansion leading to ectopic TAG accumulation.

Multiple cellular (adipocytes and non-adipocytes) and soluble components are contributors to the chronic inflammation observed in adipose during obesity development. We previously showed that recombinant LIF could increase JAK-dependent STAT3 inflammation in adipose tissue to restrict further adipose expansion when administered to wild-type and obese murine models (Arora et al., 2018, 2020). As the adipocyte-specific *STAT3* knockout model demonstrated no additional phenotypic changes beyond those observed in the adipocyte-specific *LIFR* knockout mouse, we conclude that the upstream LIFR-α component of this signaling axis is important to STAT3 adipose activation in DIO. Because we identify that IL-6 adipocyte signaling is intact in the adipocyte-specific *LIFR* knockout mouse and that we observe no difference in the phenotypes of the *LIFR* and *STAT3* adipocyte-specific null models on an HFD, our present findings

suggest that cytokines acting through LIFR-α have significant contributions to the signaling inducing STAT3 inflammation and browning in DIO that parallel IL-6.

Associations have previously been made between decreased levels of adipose expansion and increased development of NAFLD/NASH in obesity (du Plessis et al., 2015; Lotta et al., 2017; Samuel and Shulman, 2018). In the extreme metabolic setting of congenital lipodystrophy, the inability for adipose to expand results in the ectopic accumulation of TAGs in other tissues including the liver (Hussain and Garg, 2016; Safar Zadeh et al., 2013). In the setting of insulin resistance, NAFLD evolves from hepatic intrinsic and extrinsic signaling events, the latter state represented by decreased insulin-mediated suppression of lipolysis that sequentially leads to adipose expansion and eventually ectopic accumulation of liver TAGs (Samuel and Shulman, 2018; Shulman, 2000; Titchenell et al., 2017; Utzschneider and Kahn, 2006). These models center on a dysfunctional adipocyte resulting in greater TAG lipolysis than synthesis resulting in the accumulation of liver TAGs from the periphery. This is consistent with studies in which wild-type mice on an HFD generate products of increased peripheral adipocyte lipolysis that directly contribute to ectopic liver TAG accumulation (Duarte et al., 2014). Our adipocyte-specific *LIFR* knockout mouse model had similar glucose and insulin responsiveness at time points in which there were significant differences in adipose expansion and liver TAG accumulation when compared with the littermate controls, suggesting that LIFR-α/JAK/STAT3 adipose inflammatory signals promote adipocyte lipolysis and browning that directly leads to NAFLD development. We therefore suggest that, like insulin resistance, the LIFR-α/JAK/STAT3 inflammatory mechanism of blocking adipose expansion and subsequent increased NAFLD revolves around regulation of the overall adipocyte lipolysis potential. However, whereas the insulin-resistant state increases net lipolysis via release of insulin-mediated lipolysis suppression, we predict that the IL-6 family of cytokines directly increases basal lipolysis via JAK/STAT3 signaling.

A recent study suggested that catecholamines decrease adipose fatty acid re-esterification in a STAT3/GPAT-dependent mechanism increasing adipocyte oxidative metabolism (Reilly et al., 2020). Our findings highlight a different pathway, one that is driven by cytokine signaling of the LIFR-α inflammation axis in adipocytes to promote lipolysis and browning in a JAK-dependent manner (Arora et al., 2020), unlike catecholamine processing of STAT3. Although their use of a *Adipoq-Cre;STAT3*$^{fl/fl}$ mouse model on an HFD demonstrated increased adipose mass and body weight similar to our adipocyte-specific *STAT3* model on an HFD, their study did not identify differences in liver TAGs between the knockout model and littermate controls. This may be attributable to mice in their cohorts being assessed only after average body weights exceeded 58 g, a level of adipose mass after which our adipocyte-specific *STAT3* knockout model displayed no further adipose expansion resulting in increased liver TAGs at similar levels to littermate controls. As our adipocyte-specific *LIFR* and *STAT3* models on HFD had similar phenotypes, we conclude that signaling through LIFR-α alters STAT3 activation to promote lipolysis, but this signaling could also influence catecholamine signaling and suppression of fatty acid re-esterification in contributing to the overall decrease in adipose expansion.

Our findings highlight a crucial role for the adipocyte LIFR-α/JAK/STAT3 signaling axis in regulating adipose expansion and obesity-associated comorbidities of insulin resistance and NAFLD in mice under the metabolic stress of an HFD. This axis achieves such control by being a gatekeeper of adipocyte inflammatory signaling and lipolysis in DIO. Monitoring the activation of the LIFR-α axis in adipose could also allow us to predict when a patient with obesity is on the verge of forfeiting adipocyte function due to elevated adipose LIFR-α/JAK/STAT3 signaling, leading to enhanced lipolysis peripherally, and subsequently NAFLD. Inhibiting the LIFR-α/JAK/STAT3 axis in obesity could potentially block adipocyte lipolysis with subsequent adipose expansion decreasing NAFLD while maintaining insulin responsiveness.

Limitations of the study

Our *in vitro* and in *vivo* analyses demonstrated the importance of LIFR-α and STAT3 in limiting adipose expansion resulting in hepatic triacylglyceride accumulation in murine DIO models. Although murine models are suitable to study human disease processes, some disease mechanisms in the murine model do not completely overlap with those found in human disease. Our lipolysis data were performed on differentiated adipocytes derived from the SVF of adipose tissue from our genetic models. Although this an accepted *in vitro* model to study adipocyte function, the findings from these models do not always correlate with *in vivo* function.

Resource availability

Lead contact

Further information and requests for resources and reagents should be directed to and will be fulfilled by the lead contact, Rodney E. Infante (rodney.infante@utsouthwestern.edu).

Material availability

All unique reagents generated in this study will be available form the lead contact.

Data and code availability

This study did not generate large datasets.

METHODS

All methods can be found in the accompanying transparent methods supplemental file.

SUPPLEMENTAL INFORMATION

Supplemental information can be found online at https://doi.org/10.1016/j.isci.2021.102227.

ACKNOWLEDGMENTS

We thank Michael Brown, Joseph Goldstein, Jay Horton, Philipp Scherer, and Rana Gupta for their valuable suggestions. We thank Dorothy Williams for excellent technical work. This work was supported by the Burroughs Wellcome Fund Career Awards for Medical Scientists (1019692); American Gastroenterological Association Scholar Award (2019AGARSA3); Hartwell Foundation Fellowship Grant, American Cancer Society grant (133889-RSG-19-195-01-TBE); Cancer Prevention and Research Institute of Texas (RP200170); V Foundation Scholar Award (V2019-014); and National Institutes of Health grants (5P01-HL20948, P30CA142543, and 5T32GM007062-44).

AUTHOR CONTRIBUTIONS

T.G. and A.G. contributed equally. T.G., A.G., J.Z.G., A.Y.G., and J.Y. performed experiments. A.G. generated the mouse models. J.Y. generated differentiated adipocytes from genetic mouse models. A.Y.G. performed statistical analysis. B.M.E. performed pathology evaluation. T.G., A.G., J.Z.G., A.Y.G., J.Y., P.I., and R.E.I. were involved in experimental designs and data interpretation. P.I. and R.E.I. wrote the manuscript. All authors reviewed and revised the manuscript.

DECLARATION OF INTERESTS

T.G., A.G., J.Z.G., J.Y., A.Y.G., B.M.E., and P.I. acknowledge no conflicts of interest related to this work. Pfizer, Inc., is currently supporting a collaborative project with the R.E.I. laboratory that is independent of all data presented in this manuscript.

Received: November 2, 2020
Revised: February 2, 2021
Accepted: February 19, 2021
Published: March 19, 2021

REFERENCES

Arner, P. (1976). Relationship between intracellular cyclic AMP and lipolysis in human adipose tissue. Acta Med. Scand. *200*, 179–186.

Arora, G.K., Gupta, A., Guo, T., Gandhi, A.Y., Laine, A., Williams, D.L., Ahn, C., Iyengar, P., and Infante, R.E. (2020). Janus kinase inhibitors suppress cancer cachexia-associated anorexia and adipose wasting in mice. JCSM Rapid Commun. *3*, 115–128.

Arora, G.K., Gupta, A., Narayanan, S., Guo, T., Iyengar, P., and Infante, R.E. (2018). Cachexia-associated adipose loss induced by tumor-secreted leukemia inhibitory factor is counterbalanced by decreased leptin. JCI Insight *3*, e121221.

Auernhammer, C.J., and Melmed, S. (2000). Leukemia-inhibitory factor-neuroimmune modulator of endocrine function. Endocr. Rev. *21*, 313–345.

Bischoff, S.C., Boirie, Y., Cederholm, T., Chourdakis, M., Cuerda, C., Delzenne, N.M., Deutz, N.E., Fouque, D., Genton, L., Gil, C., et al. (2016). Towards a Multidisciplinary Approach to Understand and Manage Obesity and Related Diseases (Clinical nutrition).

Cernkovich, E.R., Deng, J., Bond, M.C., Combs, T.P., and Harp, J.B. (2008). Adipose-specific disruption of signal transducer and activator of transcription 3 increases body weight and adiposity. Endocrinology *149*, 1581–1590.

Cohen, J.C., Horton, J.D., and Hobbs, H.H. (2011). Human fatty liver disease: old questions and new insights. Science *332*, 1519–1523.

du Plessis, J., van Pelt, J., Korf, H., Mathieu, C., van der Schueren, B., Lannoo, M., Oyen, T., Topal, B., Fetter, G., Nayler, S., et al. (2015). Association of adipose tissue inflammation with histologic severity of nonalcoholic fatty liver disease. Gastroenterology *149*, 635–648.e614.

Duarte, J.A., Carvalho, F., Pearson, M., Horton, J.D., Browning, J.D., Jones, J.G., and Burgess, S.C. (2014). A high-fat diet suppresses de novo lipogenesis and desaturation but not elongation and triglyceride synthesis in mice. J. lipid Res. *55*, 2541–2553.

Eslam, M., Sanyal, A.J., and George, J. (2020). MAFLD: a consensus-driven proposed nomenclature for metabolic associated fatty liver disease. Gastroenterology *158*, 1999–2014.e1991.

Ferrante, A.W., Jr. (2013). The immune cells in adipose tissue. Diabetes Obes. Metab. *15* (*Suppl 3*), 34–38.

Han, M.S., White, A., Perry, R.J., Camporez, J.P., Hidalgo, J., Shulman, G.I., and Davis, R.J. (2020). Regulation of adipose tissue inflammation by interleukin 6. Proc. Natl. Acad. Sci. U S A *117*, 2751–2760.

Hussain, I., and Garg, A. (2016). Lipodystrophy syndromes. Endocrinol. Metab. Clin. North Am. *45*, 783–797.

Kosteli, A., Sugaru, E., Haemmerle, G., Martin, J.F., Lei, J., Zechner, R., and Ferrante, A.W., Jr. (2010). Weight loss and lipolysis promote a dynamic immune response in murine adipose tissue. J. Clin. Invest. *120*, 3466–3479.

Lotta, L.A., Gulati, P., Day, F.R., Payne, F., Ongen, H., van de Bunt, M., Gaulton, K.J., Eicher, J.D., Sharp, S.J., Luan, J., et al. (2017). Integrative genomic analysis implicates limited peripheral adipose storage capacity in the pathogenesis of human insulin resistance. Nat. Genet. *49*, 17–26.

Lumeng, C.N., Bodzin, J.L., and Saltiel, A.R. (2007a). Obesity induces a phenotypic switch in adipose tissue macrophage polarization. J. Clin. Invest. *117*, 175–184.

Lumeng, C.N., DelProposto, J.B., Westcott, D.J., and Saltiel, A.R. (2008). Phenotypic switching of adipose tissue macrophages with obesity is generated by spatiotemporal differences in macrophage subtypes. Diabetes *57*, 3239–3246.

Lumeng, C.N., Deyoung, S.M., Bodzin, J.L., and Saltiel, A.R. (2007b). Increased inflammatory properties of adipose tissue macrophages recruited during diet-induced obesity. Diabetes *56*, 16–23.

Metcalf, D. (1991). The leukemia inhibitory factor (LIF). Int. J. Cel. Cloning *9*, 95–108.

Milano, W., De Biasio, V., Di Munzio, W., Foggia, G., and Capasso, A. (2020). Obesity: the new global epidemic. Pharmacological treatment, opportunities and limits for personalized therapy. Endocr. Metab. Immune Disord. Drug Targets *20*, 1232–1243.

Oñate, B., Vilahur, G., Camino-López, S., Díez-Caballero, A., Ballesta-López, C., Ybarra, J., Moscatiello, F., Herrero, J., and Badimon, L. (2013). Stem cells isolated from adipose tissue of obese patients show changes in their transcriptomic profile that indicate loss in stemcellness and increased commitment to an adipocyte-like phenotype. BMC Genomics *14*, 625.

Reilly, S.M., Hung, C.W., Ahmadian, M., Zhao, P., Keinan, O., Gomez, A.V., DeLuca, J.H., Dadpey, B., Lu, D., Zaid, J., et al. (2020). Catecholamines suppress fatty acid re-esterification and increase oxidation in white adipocytes via STAT3. Nat. Metab. *2*, 620–634.

Reilly, S.M., and Saltiel, A.R. (2017). Adapting to obesity with adipose tissue inflammation. Nat. Rev. Endocrinol. *13*, 633–643.

Roytblat, L., Rachinsky, M., Fisher, A., Greemberg, L., Shapira, Y., Douvdevani, A., and Gelman, S. (2000). Raised interleukin-6 levels in obese patients. Obes. Res. *8*, 673–675.

Safar Zadeh, E., Lungu, A.O., Cochran, E.K., Brown, R.J., Ghany, M.G., Heller, T., Kleiner, D.E., and Gorden, P. (2013). The liver diseases of lipodystrophy: the long-term effect of leptin treatment. J. Hepatol. *59*, 131–137.

Samuel, V.T., and Shulman, G.I. (2018). Nonalcoholic fatty liver disease as a nexus of metabolic and hepatic diseases. Cell Metab. *27*, 22–41.

Seto, D.N., Kandarian, S.C., and Jackman, R.W. (2015). A key role for leukemia inhibitory factor in C26 cancer cachexia. J. Biol. Chem. *290*, 19976–19986.

Shulman, G.I. (2000). Cellular mechanisms of insulin resistance. J. Clin. Invest. *106*, 171–176.

Song, H., and Lim, H. (2006). Evidence for heterodimeric association of leukemia inhibitory factor (LIF) receptor and gp130 in the mouse uterus for LIF signaling during blastocyst implantation. Reproduction *131*, 341–349.

Tamm, C., Böwer, N., and Annerén, C. (2011). Regulation of mouse embryonic stem cell self-renewal by a Yes-YAP-TEAD2 signaling pathway downstream of LIF. J. Cell Sci. *124*, 1136–1144.

Titchenell, P.M., Lazar, M.A., and Birnbaum, M.J. (2017). Unraveling the regulation of hepatic metabolism by insulin. Trends Endocrinol. Metab. *28*, 497–505.

Utzschneider, K.M., and Kahn, S.E. (2006). Review: the role of insulin resistance in nonalcoholic fatty liver disease. J. Clin. Endocrinol. Metab. *91*, 4753–4761.

Van Pelt, D.W., Guth, L.M., Wang, A.Y., and Horowitz, J.F. (2017). Factors regulating subcutaneous adipose tissue storage, fibrosis, and inflammation may underlie low fatty acid mobilization in insulin-sensitive obese adults. Am. J. Physiol.Endocrinol. Metab. *313*, E429–e439.

Vaughan, M., and Steinberg, D. (1963). Effect of hormones on lipolysis and esterification of free fatty acids during incubation of adipose tissue in vitro. J. Lipid Res. *4*, 193–199.

Ware, C.B., Horowitz, M.C., Renshaw, B.R., Hunt, J.S., Liggitt, D., Koblar, S.A., Gliniak, B.C., McKenna, H.J., Papayannopoulou, T., Thoma, B., et al. (1995). Targeted disruption of the low-affinity leukemia inhibitory factor receptor gene causes placental, skeletal, neural and metabolic defects and results in perinatal death. Development *121*, 1283–1299.

Yeste, D., Vendrell, J., Tomasini, R., Broch, M., Gussinyé, M., Megia, A., and Carrascosa, A. (2007). Interleukin-6 in obese children and adolescents with and without glucose intolerance. Diabetes care *30*, 1892–1894.

Yin, W., Mu, J., and Birnbaum, M.J. (2003). Role of AMP-activated protein kinase in cyclic AMP-dependent lipolysis in 3T3-L1 adipocytes. J. Biol. Chem. *278*, 43074–43080.

iScience, Volume *24*

Supplemental information

LIFR-α-dependent adipocyte signaling in obesity limits adipose expansion contributing to fatty liver disease

Tong Guo, Arun Gupta, Jinhai Yu, Jorge Z. Granados, Aakash Y. Gandhi, Bret M. Evers, Puneeth Iyengar, and Rodney E. Infante

SUPPLEMENTAL INFORMATION

Supplemental Text and Figures

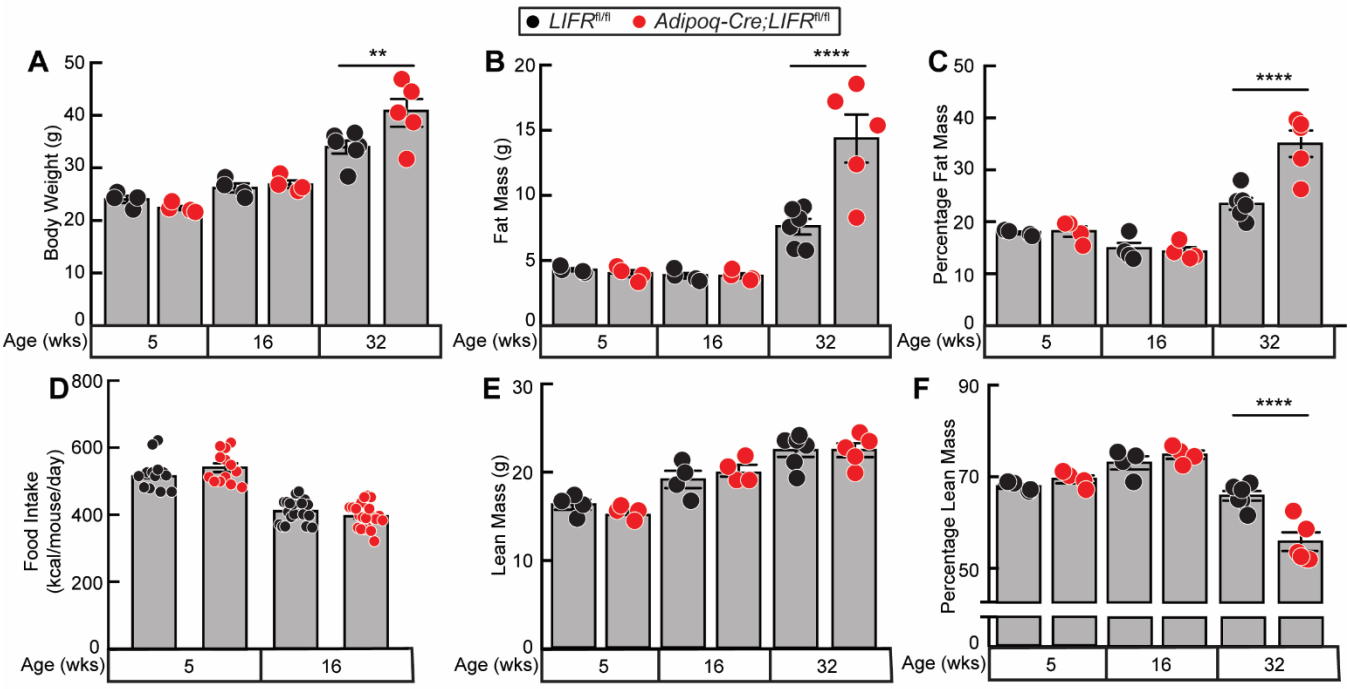

Figure S1. Development of *Adipoq-Cre;LIFR$^{fl/fl}$* Mouse Model, related to Figure 2. A-F) *LIFR$^{fl/fl}$* and *Adipoq-Cre;LIFR$^{fl/fl}$* male mice at 5-weeks (n=4), 16-weeks (n=4), and 32-weeks (n=5-6) of age on a regular chow diet were evaluated for body weight (A), adipose mass by ECHO MRI (B), and lean mass by ECHO MRI (E). Percentage of fat mass (C) and lean mass (F) were calculated per body weight. Mice were also followed for two weeks to monitor food intake (D). Data are shown as mean ± SEM. ****p<0.001 and ****p<0.0001* based on a two-way ANOVA with Sidak's multiple comparison tests comparing *LIFR$^{fl/fl}$* to *Adipoq-Cre;LIFR$^{fl/fl}$* cohorts.

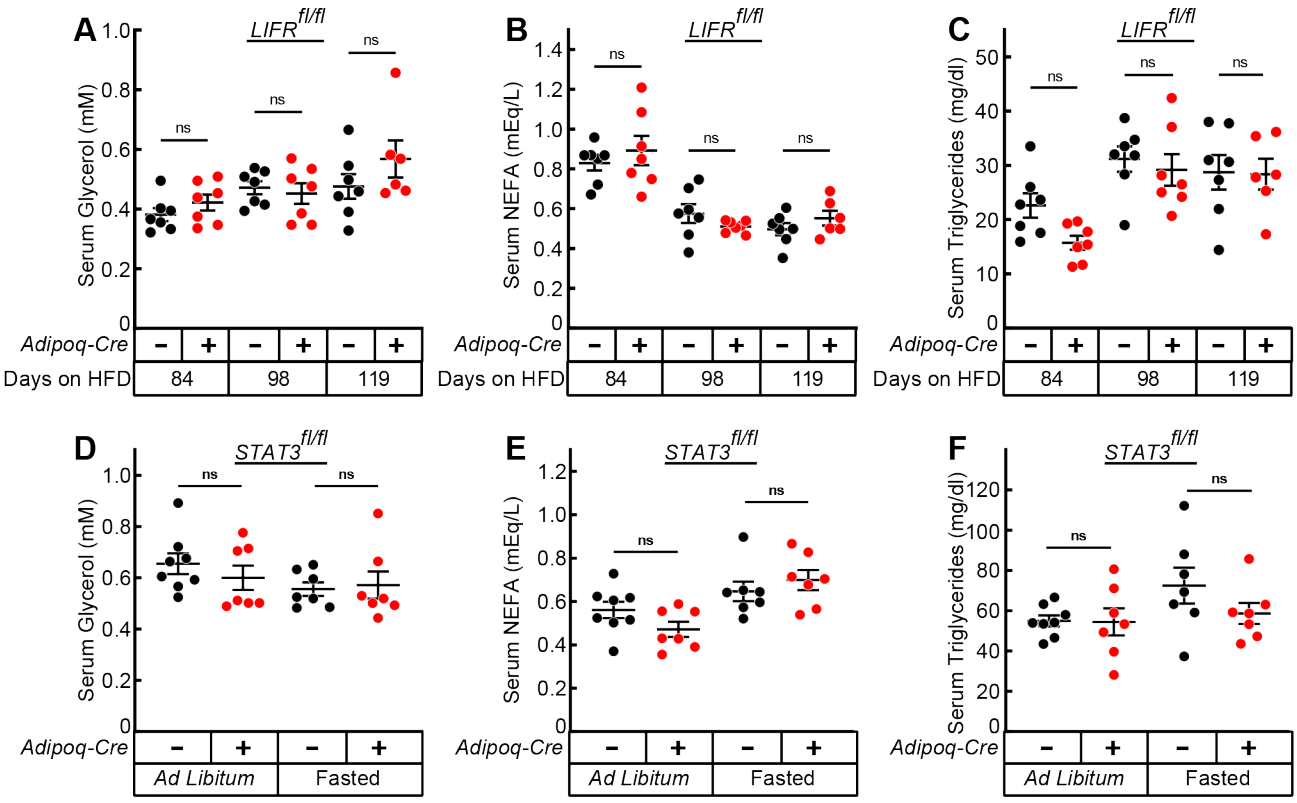

Figure S2. Serum Lipid and Lipolysis Markers in Genetic Models on High Fat Diet, related to Figure 3 and Figure 7. A-C) *LIFR*$^{fl/fl}$ and *Adipoq-Cre;LIFR*$^{fl/fl}$ male mice (n=7) at 7-weeks of age were started on a high fat diet and serum was obtained on the indicated days after a 5 h fast. D-F) *STAT3*$^{fl/fl}$ and *Adipoq-Cre;STAT3*$^{fl/fl}$ male mice (n=7-8) at 9-weeks of age were started on a high fat diet and serum was obtained after 100 days (*Ad Libitum*) and 105 days after a 5 h fast (*Fasted*). A-F) Serum glycerol (A,D), non-esterified fatty acids (B,E), and triacylglycerides (C,F) were quantified as described in *STAR*Methods*. Data are shown as dot plots with mean ± SEM. *ns* = *non-significant* based on a two-way ANOVA with Sidak's multiple comparison tests comparing with and without *Adipoq-Cre* cohorts.

Transparent Methods

KEY RESOURCES TABLE

REAGENT	SOURCE	IDENTIFIER
Antibodies		
Mouse monoclonal anti-β-Actin	Cell Signaling Technology	Cat# 3700
Mouse monoclonal anti-STAT3	Cell Signaling Technology	Cat# 9139
Mouse monoclonal anti-pSTAT3	Cell Signaling Technology	Cat# 9138
Rabbit polyclonal anti-LIFR	Proteintech Group, Inc.	Cat# 22779-1-AP
Peroxidase AffiniPure Donkey Anti-Mouse IgG a	Jackson ImmunoResearch	Cat# 715-035-150
Peroxidase AffiniPure Goat Anti-Rabbit IgG	Jackson ImmunoResearch	Cat# 111-035-003
Chemicals and Recombinant Proteins		
Precision Plus Protein Kaleidoscope Standards	BioRad, Inc	Cat# 1610375
protease inhibitor cocktail	Calbiochem	Cat# 539131
Insulin Solution	Cayman	Cat# 10008979
Fetal Bovine Serum (FBS)	Corning	Cat# 35-015-CV
DMEM/F12	Corning	Cat# 10-090-CV
phosphatase inhibitor cocktail Set I	EMD Millipore	Cat# 524624
phosphatase inhibitor cocktail Set II	EMD Millipore	Cat# 524625
Penicillin-Streptomycin Solution	Gibco	Cat# 15140122
rIL-6	PeproTech	Cat# 216-16
Collagenase D	Roche	Cat#11088882001
Bovine serum albumin (BSA), molecular biology grade (for primary antibody dilutions)	RPI	Cat# A30075
High Fat Diet	Research Diets	Cat# 12492
Bovine serum albumin (BSA), fatty-acid free (for cell culture media)	Sigma	Cat# A7030
Chloroform	Sigma	Cat# 372978
Dexamethasone	Sigma	Cat# D4902
DMEM with high glucose	Sigma	Cat# CD6429
Dulbecco's Phosphate Buffered Saline (DPBS)	Sigma	Cat# D8537
Free Glycerol Reagent	Sigma	Cat# F6428
Glycerol Standard Solution	Sigma	Cat# G7793
Glucose	Sigma	Cat# G7021-100G
HBSS buffer	Sigma	Cat# H8264
3-isobutyl-1-methylxanthine	Sigma	Cat# I5879-5G
Isoproterenol	Sigma	Cat# I6504
NKH477	Sigma	Cat# N3290
Serum Triglyceride Determination Kit	Sigma	Cat# TR0100
Rosiglitazone	Sigma	Cat# R2408-50MG
Chow Diet	Teklad	Cat# 7912
RNA-STAT-60	Tel-Test	Cat# CS-111
DMEM without glucose	Thermo	Cat# A1443001

SuperSignal™ West Pico PLUS Chemiluminescent Substrate	Thermo Scientific	Cat# 34580
Critical Commercial Assays		
RNeasy Mini Kit	Qiagen	Cat# 74106
Pierce™ Bicinchoninic Acid Kit	Thermo Scientific	Cat# 23225
NEFA-HR Color Reagent A	Wako Diagnostics	Cat# 999-34691
NEFA-HR Solvent A	Wako Diagnostics	Cat# 995-34791
NEFA-HR Color Reagent B	Wako Diagnostics	Cat# 991-34891
NEFA-HR Solvent B	Wako Diagnostics	Cat# 993-35191
NEFA-HR NEFA Standard Solution	Wako Diagnostics	Cat# 276-76491
Experimental Models: Mouse strains		
C57BL/6N-Atm1Brd/a Lifrtm1a	Mutant Mouse Resource & Research Center at UC Davis	Cat# 037850-UCD
B6.Cg-Tg(Pgk1-flpo)10Sykr/J	The Jackson Laboratory	Cat# 011065
B6.129S1-Stat3tm1Xyfu/J	The Jackson Laboratory	Cat# 016923
B6.FVB-Tg(Adipoq-Cre)1Evdr/J	The Jackson Laboratory	Cat# 016923

RESOURCE AVAILABILITY

Lead Contact

Further information and requests for reagents and resources can be directed to the Lead Contact, Rodney Infante (rodney.infante@utsouthwestern.edu).

Materials Availability

All materials and mice generated in this study are available from the Lead Contact.

DATA AND CODE AVAILABILITY

No large datasets were derived from these experiments

EXPERIMENTAL MODEL and SUBJECT DETAILS

Animal Details

Conditional-ready *LIFR*$^{fl/fl}$ mice were created by crossing the *C57BL/6N-Atm1Brd/a Lifrtm1a* (Mutant Mouse Resource & Research Center at UC Davis) with the *B6.Cg-Tg(Pgk1-flpo)10Sykr/J* (Jackson Laboratory) to remove the Flp-recombination cassette. *Adipoq-Cre-LIFR*$^{fl/fl}$ were created by crossing female conditional-ready *LIFR*$^{fl/fl}$ mice with male *B6.FVB-Tg(Adipoq-cre)1Evdr/J* (Jackson Laboratory). Adipocyte-specific deletion of *LIFR* was confirmed by post recombination genomic PCR, qPCR of mRNA, and immunoblot analysis for protein expression. Genomic PCR protocols for genotyping *LIFR* were provided by Mutant Mouse Resource & Research Center at UC Davis. Adipoq-Cre specific genomic PCR protocol was obtained from Jackson Laboratory. Female *STAT3*$^{fl/fl}$ mice (Jackson Laboratory) were obtained and crossed with *B6.FVB-Tg(Adipoq-Cre)1Evdr/J* (Jackson Laboratory) to generate *Adipoq-Cre-STAT3*$^{fl/fl}$ mice. Deletion of *Stat3* gene from Adipocyte was confirmed by PCR as well as Western Blot. *Stat3* related PCR protocols were obtained from The Jackson Laboratory. Adipocyte-specific deletion of STAT3 was confirmed by post recombination genomic PCR, qPCR of mRNA, and immunoblot analysis for protein expression. Genotyping was performed by PCR of genomic DNA obtained from the

tails, ears, or the indicated tissues. The primer sequences from Integrated DNA Technologies used for PCR were as follows:

Name	Sequence
LIFR-37850-F	CTGCTCCTGGAAGACACATGAGC
LIFR-37850-TTR	TGCTGGGATTAAAGGCGTGAGC
LIFR-37850-R	GACTGGGCATTTACTATATCCAAGGG
STAT3-F	ATTGGAACCTGGGACCAAGTGG
STAT3–R	GCTGGCTCATAGGCAAAAACAC
STAT3-19436-F	TTG ACC TGT GCT CCT ACA AAA A
STAT3-19437-R	CCC TAG ATT AGG CCA GCA CA
AdipoqCre-15381-F	ACG GAC AGA AGC ATT TTC CA
AdipoqCre-18564-R	GGA TGT GCC ATG TGA GTC TG

All mice were allowed to acclimate in UT Southwestern animal facilities. Animals were kept in a temperature-controlled facility with a 12 h light/dark cycle and were fed regular chow diet or high fat diet (60% fat calories). At the end of the experiments, mice were euthanized at the indicated time point as recommended by the Institutional Animal Care and Use Committee by using a CO2 chamber, and organs were collected for formalin fixation or snap frozen for genomic, protein expression, or lipid analysis. All animal studies were conducted under an Institutional Animal Care and Use Committee approved protocol at UT Southwestern Medical Center (Dallas, Texas). Body weight was measured using a standard balance (digital Ohaus scale). Adipose tissue mass and lean tissue mass were measured longitudinally using ECHO MRI (ECHO Medical Systems) at 9AM at the indicated time points. Food intake was measured as previously described (Arora et al., 2018). For metabolic cage studies, animals were evaluated using CLAMS in the UT Southwestern Medical Center Metabolic Phenotyping Core Facility. Glucose tolerance test (GTT) and insulin tolerance test (ITT) were performed on the indicated time points after fasting mice overnight. GTT was performed with I.P. injection of 2 g glucose per kg body weight dissolved in PBS. Injection volume was calculated based on 5 μl per gram body weight. ITT was performed with I.P. injection of 0.1 U/ml insulin (regular chow diet, day 0) or 0.2 U/ml insulin (high fat diet) per kg body weight dissolved in PBS. Blood glucose levels were measured at the indicated time points using glucose meters (Contour). Serum glycerol concentration was measured by using 20 μl of serum in our glycerol assay previously described (Arora et al., 2018). Serum NEFA (Wako Diagnostics) and triacylglycerides (Sigma) were measured as per the manufacture's instructions.

Method Details

Immunoblot Analysis

Immunoblot analysis of tissues or cells were processed as described previously (Arora et al., 2018). Primary antibodies for these studies were: IgG-LIFR (1:1000 dilution) IgG-Actin (1:10000 dilution), IgG-STAT3 (1:1000 dilution), and IgG-pSTAT3 (1:1000 dilution).

Adipocyte Fractionation

Epididymal white adipose tissue (4 depots from two mice) was minced and incubated in 10ml of HBSS buffer containing 1mg/ml collagenase D and 1.5% BSA (fatty acid free) in a 37 °C water bath with shaking for 50 min. The cell mixture was passed through a 100-µm cell strainer (Cat# 352360, Falcon), and the filtrate was combined with 10 ml of DPBS containing 2% FCS. After centrifugation at 600 *g* for 5 min, the lipid layer/fat cake was transferred to a 1.7 mL tube for immunoblot and qPCR analysis.

Isolation of Murine Stromal-Vascular Fraction and Differentiation to Adipocytes

Inguinal white adipose tissue (~0.5 g) from 6-8 week-old mice were minced and incubated in 25 ml of HBSS buffer containing 1 mg/ml collagenase D and 1.5% BSA (fatty acid free) in a 37 °C water bath with shaking for 50 min. The cell mixture was passed through a 100-µm cell strainer (Cat# 352360, Falcon), and the filtrate was combined with 25 ml of DPBS containing 2% FBS. After centrifugation at 600 *g* for 5 min, the lipid layer/fat cake and supernatant were removed by aspiration. After the pellet was resuspended in 1 ml red blood cell lysis buffer (155 mM NH_4Cl, 12 mM $NaHCO_3$, 0.1 mM EDTA) and incubated for 2 min, it was supplemented with 5 ml DPBS containing 2% FBS. The cell mixture was passed through a 40-µm cell strainer (Cat# 352340, Falcon), and the filtrate we combined with 6 ml of DPBS containing 2% FBS. After centrifugation at 600 *g* for 5 min, the cell pellet was resuspended in 20 ml of DMEM/F12 medium supplemented with 10% FBS, 10 U/ml penicillin and 10 U/ml streptomycin (growth medium) and then plated equally into two 10-cm dishes and maintained in monolayer culture at 37°C in 10% CO_2. Starting the next day, the medium was aspirated, and 10 ml of fresh growth medium was added every other day until the cells reached ~50 % confluence. At this point, medium was aspirated, and washed two times with 8 ml DPBS, and each dish was supplemented with 1.5 ml of Trypsin-EDTA solution containing 0.25% trypsin (Cat# T4049, Sigma) for 5 min followed by supplementation with 8 ml of growth medium. After centrifugation at 400 *g* for 5 min, resuspended cells with 10 ml growth medium, approximately 2.5 ml cell suspension was placed into 10-cm dishes supplemented with 7.5 ml of growth medium to maintain the line, and the rest 7.5 ml cell suspension were plated per well into a 12-well plate for differentiation. Differentiation was induced with culture medium supplemented with 0.11 mg/ml 3-isobutyl-1-methylxanthine, 0.1 µg/ml dexamethasone, 1:1000 insulin solution and 1 µM rosiglitazone for 4 days, followed by DMEM high glucose medium with 10% FBS, 10 U/ml penicillin and 10 U/ml streptomycin for 3 or 4 days. Cells were used for experiments at 7 or 8 day since the induction. Only cells with differentiation rate higher than 80% were used.

Lipolysis (Glycerol Release/NEFA Release)

Only day 7-8 differentiated adipocytes in a 12-well format with a minimum of 80% differentiation were used for assays. Medium was removed from each well containing differentiated adipocytes, and cells were washed with 1 ml of PBS 2 times. Adipocytes were supplemented with 1 ml DMEM without glucose supplemented with 0.4% fatty acid free BSA and10 mM glucose, 10 U/ml penicillin and 10 U/ml streptomycin containing 2 µl of DMSO or 2 µl of PBS in the absence or presence of the indicated concentration of isoproterenol, NKH477, LIF, or IL-6 for 20 h followed by collection of cells for immunoblot analysis and medium to quantify glycerol and NEFA. Media glycerol concentration from differentiated adipocytes was measured for each condition in triplicate as previously described (Arora et al., 2018). Media non-esterified fatty acid (NEFA) concentration from differentiated adipocytes was measured per manufacture directions of the commercially available NEFA assay kit. Briefly, 20 µl of medium from the differentiated adipocytes were aliquoted into a 96-well plate containing standards followed by supplementation of 100 ul of Reagent A of the NEFA assay kit. After the plate was placed on a shaker at room temperature for 30 s, it was incubated at 37 °C for 5 min followed by measurement of absorbance (wavelength 550 nm) using a BioTek microplate reader (Synergy H1). Then, each well of the 96-well plate was supplemented with 50 µl of Reagent B of the NEFA assay kit. After the plate was placed on a shaker at room temperature for 30 s, it was incubated at 37 °C for 5 min followed by another measurement

of absorbance (wavelength 550 nm) using a BioTek microplate reader. The amount of NEFA concentration released into the medium per condition over background was calculated using the formula described in the U Cinn - *NEFA Concentration protocol on the National Mouse Metabolic Phenotyping Centers* website (https://www.mmpc.org/shared/protocols.aspx). Recombinant LIF used in lipolysis assays was purified as previously described (Arora et al., 2018).

Histopathology

Histological sections (5 μm) were cut from paraffin-embedded eWAT or liver, mounted on glass slides, and dried overnight at 37 °C. Digital images were captured using an Aperio CS2 scanner (Leica Biosystems Inc., Buffalo Grove, IL) at 4x, 10X, and 20x magnification. A blinded pathologist reviewed and interpreted the findings of the eWAT and/or liver H&E sections for each animal of every cohort. For experiments quantifying adipocyte diameter, computerized morphometric analysis of individual adipocytes was performed using Image J software (NIH) of slides at 20X magnification. The diameter of 50 adipocytes from one 10X representative H&E field per slide was analyzed for each animal in the cohort.

Determination of Hepatic Triacylglyceride and Cholesterol Contents

Frozen liver tissues (100-200 mg) was used for extractions by the UT Southwestern Medical Center Metabolic Phenotyping Core Facility for liver triacylglycerides and cholesterol quantification.

Real-time PCR analysis of gene expression

For quantitative real-time PCR (qRT-PCR) of adipose depots or isolated adipocytes from eWAT for the indicated gene products were conducted as previously described (Arora et al.). The primer sequences from Integrated DNA Technologies used for PCR in these studies were as follows:

qRT-PCR primers		
NCBI Gene Symbol	**Primer Name (Internal Designation)**	**Sequence (5' to 3')**
Actb	mouse-bactin-Forward	CCGTGAAAAGATGACCCAGATC
Actb	mouse-bactin-Reverse	CACAGCCTGGATGGCTACGT
Rps18	mouse-Rps18-Forward	CATGCAGAACCCACGACAGTA
Rps18	mouse-Rps18-Reverse	CCTCACGCAGCTTGTTGTCTA
Lifr	mouse-mLIFR-Forward	GATTTGTCTGCTGACTTCTTCAC
Lifr	mouse-mLIFR-Reverse	GAGTAACACGAGTGCTACTGG
Stat3	mouse-STAT3-Forward	TTGGAATGAAGGGTACATCATGG
Stat3	mouse-STAT3-Reverse	TCCACCCAAGTGAAAGTGAC
Gdf15	mouse-GDF15-Forward	CTCTCAACTGAGGTTCCTGC
Gdf15	mouse-GDF15-Reverse	CCAATCTCACCTCTGGACTG
IL6	mouse-IL6-Forward	TCGTGGAAATGAGAAAAGAGTTG
IL6	mouse-IL6-Reverse	AGTGCATCATCGTTGTTCATACA
Socs3	mouse-SOCS3-Forward	CACCTGGACTCCTATGAGAAAGTG
Socs3	mouse-SOCS3-Reverse	GAGCATCATACTGATCCAGGAACT
Lep	mouse-Leptin-Forward	CTCCATCTGCTGGCCTTCTC

Lep	mouse-Leptin-Reverse	CATCCAGGCTCTCTGGCTTCT
Lif	mouse-LIF-Forward	AGCCGTTTCCCAACAACGT
Lif	mouse-LIF-Reverse	CCGTTGCCATGGAAAGAT
Tnf	mouse-TNFα-Forward	CTGAGGTCAATCTGCCCAAGTAC
Tnf	mouse-TNFα-Reverse	CTTCACAGAGCAATGACTCCAAAG
Pnpla2	mouse-ATGL-Forward	GAGAGAACGTCATCATATCCCACTT
Pnpla2	mouse-ATGL-Reverse	CCACAGTACACCGGGATAAATGT
Lipe	mouse-HSL-Forward292	GGAGCACTACAAACGCAACGA
Lipe	mouse-HSL-Reverse293	TCGGCCACCGGTAAAGAG
Ucp1	mouse-UCP1-Forward	GAGGTGTGGCAGTGTTCATTG
Ucp1	mouse-UCP1-Reverse	GGCTTGCATTCTGACCTTCA
Cidea	mouse-Cidea-Forward	CCGAGTACTGGGCGATACAGA
Cidea	mouse-Cidea-Reverse	GGTTACATGAACCAGCCTTTGG
Cidec	mouse-Cidec-Forward	AAGCGCATCGTGAAGGAGAT
Cidec	mouse-Cidec-Reverse	GGTGCCAAGCAGCATGTG
Ppargc1a	mouse-PGC1-Forward	AACCACACCCACAGGATCAGA
Ppargc1a	mouse-PGC1-Reverse	TCTTCGCTTTATTGCTCCATGA
Lpl	mouse-LPL-Forward	ACTCTGTGTCTAACTGCCACTTCAA
Lpl	mouse-LPL-Reverse	ATACATTCCCGTTACCGTCCAT
Mgll	mouse-MGL-Forward	CAGAGAGGCCCACCTACTTTT
Mgll	mouse-MGL-Reverse	ATGCGCCCCAAGGTCATATTT
Gpam	mouse-GPAT1-Forward	ACAGTTGGCACAATAGACGTTT
Gpam	mouse-GPAT1-Reverse	CCTTCCATTTCAGTGTTGCAGA
Gpat2	mouse-GPAT2-Forward	CACTGCTCCGAGGTTTTGATG
Gpat2	mouse-GPAT2-Reverse	AGGTTGGCAGCAATTCCATAC
Gpat3	mouse-GPAT3-Forward	TCCTTTTACCCTCGGCCTTC
Gpat3	mouse-GPAT3-Reverse	AGAGCTCGAAGTCCCTTCCT
Gpat4	mouse-GPAT4-Forward	CACCCTGCTGCTTGTTTTCA
Gpat4	mouse-GPAT4-Reverse	TGATTCCGTTGGTGTAGGGC
Agpat1	mouse-AGPAT1-Forward	GCTGGCTGGCAGGAATCAT
Agpat1	mouse-AGPAT1-Reverse	GTCTGAGCCACCTCGGACAT
Agpat2	mouse-AGPAT2-Forward	TTTGAGGTCAGCGGACAGAA
Agpat2	mouse-AGPAT2-Reverse	AGGATGCTCTGGTGATTAGAGATGA
Agpat4	mouse-AGPAT4-Forward	ACTTCGTGGAAATGATCTTTTGC
Agpat4	mouse-AGPAT4-Reverse	GAGGTGCAGCAGGCTCTTG
Dgat1	mouse-DGAT1-Forward	GAGGCCTCTCTGCCCCTATG
Dgat1	mouse-DGAT1-Reverse	GCCCCTGGACAACACAGACT
Dgat2	mouse-DGAT2-Forward	CCGCAAAGGCTTTGTGAAG
Dgat2	mouse-DGAT2-Reverse	GGAATAAGTGGGAACCAGATCA

Statistical Analysis

Details of statistical analysis for each experiment can be found in the respective figure legend. Data is presented as mean ± SEM, dot plots ± SEM, dot plots with bars ± SEM, or histogram. For experiments with a two-group design, a one- or two-tailed unpaired Student's t-test of the means or area under curve (AUC) was used to determine the significance of experimental results. For experiments requiring multiple

t-tests, the Bonferroni-Sidak multiple test correction was applied before identifying significant differences between groups. For experiments with a two-factorial design, significance between Cre-(-) and Cre-(+) cohorts were determined by two-way analysis of variance (ANOVA) followed by the indicated multiple comparison post-test. For statistical evaluation of growth-over-time, histogram, or linear data structures, non-linear regression was used to fit the appropriate curve (logistic growth, Gaussian, or straight line, respectively) to cohorts followed by extra sum-of-squares F test to identify differences in cohort curves. For some animal studies, the robust regression and outlier removal (ROUT) method was used to identify and remove outliers. Significance was considered if $p < 0.05$. All analyses were conducted using Prism 8 (GraphPad).

REFERENCES

Arora, G.K., Gupta, A., Narayanan, S., Guo, T., Iyengar, P., and Infante, R.E. (2018). Cachexia-associated adipose loss induced by tumor-secreted leukemia inhibitory factor is counterbalanced by decreased leptin. JCI Insight *3*.